Journal of Medicinal Chemistry

pubs.acs.org/jmc

Article

7-Hydroxycoumarins Are Affinity-Based Fluorescent Probes for Competitive Binding Studies of Macrophage Migration Inhibitory Factor

Zhangping Xiao, Deng Chen, Shanshan Song, Ramon van der Vlag, Petra E. van der Wouden, Ronald van Merkerk, Robbert H. Cool, Anna K. H. Hirsch, Barbro N. Melgert, Wim J. Quax, Gerrit J. Poelarends, and Frank J. Dekker*

Cite This: J. Med. Chem. 2020, 63, 11920−11933

Read Online

ACCESS | Metrics & More | Article Recommendations | Supporting Information

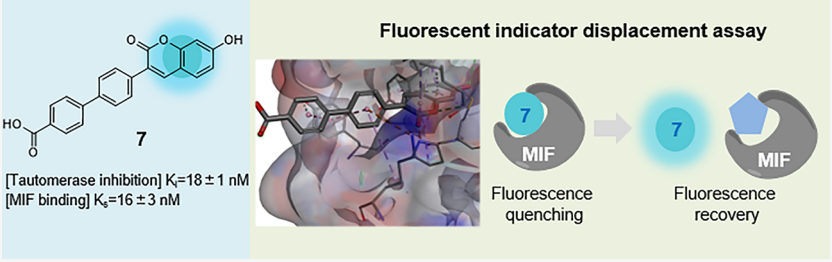

ABSTRACT: Macrophage migration inhibitory factor (MIF) is a cytokine with key roles in inflammation and cancer, which qualifies it as a potential drug target. Apart from its cytokine activity, MIF also harbors enzyme activity for keto−enol tautomerization. MIF enzymatic activity has been used for identification of MIF binding molecules that also interfere with its biological activity. However, MIF tautomerase activity assays are troubled by irregularities, thus creating a need for alternative methods. In this study, we identified a 7-hydroxycoumarin fluorophore with high affinity for the MIF tautomerase active site (K_i = 18 ± 1 nM) that binds with concomitant quenching of its fluorescence. This property enabled development of a novel competition-based assay format to quantify MIF binding. We also demonstrated that the 7-hydroxycoumarin fluorophore interfered with the MIF−CD74 interaction and inhibited proliferation of A549 cells. Thus, we provide a high-affinity MIF binder as a novel tool to advance MIF-oriented research.

INTRODUCTION

The impact of cancer as a major public health problem is demonstrated by the estimated 9.6 million cancer-related deaths worldwide in 2018.[1] Although substantial progress has been achieved over the last decades, cancer treatment remains a challenge.[2] This challenge can be addressed by exploring novel molecular mechanisms involved in cell proliferation to identify novel therapeutics. Apart from inflammation,[3,4] the cytokine macrophage migration inhibitory factor (MIF) has also been connected to several processes in the pathogenesis and progression of cancer.[5,6] Overexpression of MIF was found in several cancers, including genitourinary cancer,[7] melanoma,[8] neuroblastoma,[9] and lung carcinoma.[10] Both clinical and animal studies demonstrated that MIF enhanced tumor growth, invasion, and angiogenesis.[11,12] Additionally, MIF gene knockout or knockdown decreased proliferation and increased apoptosis of cancer cells.[13,14] The role of MIF in tumor development indicates that MIF represents a potential drug target for cancer therapy.

On a molecular level, MIF operates via protein−protein interactions (PPIs) with membrane-bound receptors such as the cluster of differentiation 74 (CD74), CXCR4, and CXCR7 receptors, as well as with intracellular targets such as p53 and Jab.[15−18] Binding of MIF to CD74 triggers activation of the mitogen-activated protein kinase (MAPK) pathway and inhibition of p53, which both suppress apoptosis and enhance cell proliferation.[7] Development of molecules that interfere with MIF−receptor interactions is an attractive strategy to inhibit MIF-induced cellular signaling. The utility of this approach has been demonstrated by the development of the MIF-neutralizing antibody imalumab, which is currently in a phase II clinical trial for treatment of patients with metastatic colorectal cancer.[19] Also, the development of small-molecule MIF binders to interfere with MIF signaling has gained attention over the past years.[20,21]

Received: July 6, 2020
Published: September 17, 2020

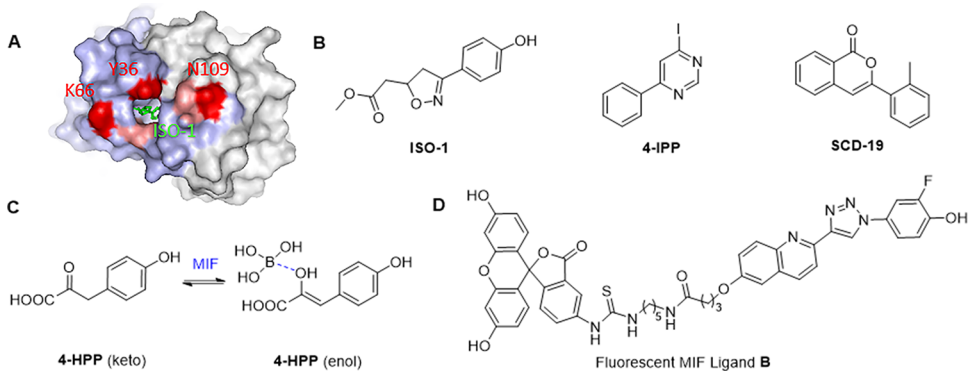

Figure 1. Structure of MIF, MIF tautomerase inhibitors, and molecules used for MIF binding studies. (A) The MIF surface alanine-scanning mutagenesis study results and ISO-1 binding site (PDB code: 1LJT[38]). The regions highlighted in red or pink show mutants that cannot or can only partially activate CD74, respectively.[24] ISO-1 is shown in green.[38] The ISO-1 binding site is located in the vicinity of amino acid residues involved in CD74 receptor activation, such as Y36, K66, and N109. (B) Structures of ISO-1,[28] 4-IPP,[31] and SCD-19.[30] (C) 4-HPP tautomerization catalyzed by MIF.[33] (D) Structure of ligand B for the fluorescence polarization probe assay.[37]

There is structural information available to facilitate development of MIF-targeted therapeutics. MIF exists in a homotrimeric form, in which each monomer contains a peptide with 114 amino acids folding into two β-strands and four α-helixes.[22] MIF also harbors three tautomerase active sites, each located at the interface between two adjacent monomers, centering around Pro1 residues,[23] that catalyze keto−enol conversion of substrates such as D-dopachrome and 4-hydroxylphenylpyruvate (4-HPP). Importantly, the enzyme active sites are located in the vicinity of amino acid residues that are involved in binding to the CD74 receptor. For instance, amino acid residues Y36, K66, N109, I64, and W108 on the MIF surface (Figure 1A) were mapped as residues responsible for activation of CD74 by alanine-scanning mutagenesis.[24] Residues 79−86 on the second α_2-helix were also identified to be responsible for MIF−CD74 binding.[25] Interestingly, Y99 of MIF was reported to regulate both catalytic activity and CD74 activation allosterically.[26] Therefore, inhibitors of MIF tautomerase activity can be expected to interfere with MIF/CD74 binding and MIF-induced signaling.[27] The initially discovered MIF tautomerase inhibitor ISO-1 (Figure 1B) also suppresses MIF cytokine activity.[28] For instance, ISO-1 significantly inhibited prostate cancer growth through neutralizing MIF-triggered MAPK pathway activation both on the cellular level and in animal models.[29] Other inhibitors like 4-IPP and SCD-19 (Figure 1B) were also effective in inhibition of MIF-mediated tumor cell growth or migration.[30,31] However, the currently available inhibitors are not in clinical development for various reasons, such as the lack of potency, poor physicochemical properties, chemical reactivity, *etc.* Therefore, novel inhibitors with improved properties are needed to facilitate both basic research and drug development.

Several assays have been developed to study binding to the MIF tautomerase active site. The most commonly used assay format depends on MIF-catalyzed keto−enol tautomerization of D-dopachrome methyl ester or 4-HPP that can be monitored by a corresponding change in the UV absorption spectrum (Figure 1C). Despite its utility, this tautomerization-based assay format has several drawbacks. The use of D-dopachrome methyl ester has the disadvantage that it can undergo spontaneous decarboxylation to form 5,6-dihydroxyindole (DHI) and CO_2,[32] which makes this substrate less convenient. The substrate 4-HPP proved to be a more stable substrate for MIF-catalyzed tautomerization,[33] which stimulated broad application in MIF tautomerase activity assays. Nevertheless, the 4-HPP enol reaction product proved to be relatively unstable in an aqueous environment for both enthalpic and entropic reasons.[34] This creates the need to perform the MIF-catalyzed tautomerization of 4-HPP in buffers with relatively low pH (~6.0) and high concentrations of boric acid and ammonium acetate to stabilize the enol reaction product. We also note that the UV absorbance at 306 nm for detection of the 4-HPP enol reaction product is relatively unspecific, which increases the chance for interference by UV-active compounds. These and other factors can result in irregularities in MIF tautomerase enzyme activity assays as described previously.[35,36] This demonstrates the need for complementary assays to study MIF binding such as the fluorescence polarization competition assay with fluorescently labeled MIF ligand B as shown in Figure 1D.[37] Here, we provide a fluorescent indicator displacement (FID) assay as a convenient and sensitive assay for MIF binding studies.

The FID assay provides a convenient format for competitive binding studies.[39,40] In this assay format, a fluorescent indicator is allowed to bind reversibly to a receptor upon which binding of a competing ligand can be quantified by displacement of the fluorescent indicator.[41] Development of a fluorescent indicator that binds tightly to the target and changes fluorescence upon binding is key to successful development of an FID assay. We envisioned that 7-hydroxycoumarin derivatives are promising fluorophores for the development of a fluorescent MIF-binding sensor because of their intensive fluorescence.[42] Importantly, these fluorophores were reported to bind to the MIF tautomerase active site.[43] However, their utility in an FID assay for MIF has not yet been explored.

In this study, we describe the development of a 7-hydroxycoumarin inhibitor as a fluorescent indicator for an FID assay to study binding to the MIF tautomerase active site. Toward this aim, a series of 7-hydroxycoumarins were synthesized and the structure−activity relationships (SARs) for MIF binding and concomitant fluorescence quenching were explored. A 7-hydroxycoumarin derivative with nanomolar potency was identified and used for the development of a convenient and sensitive FID assay for MIF binder assessment. Furthermore, we also explored the 7-hydroxycoumarin inhibitor for its potency to interfere with the MIF−CD74

https://dx.doi.org/10.1021/acs.jmedchem.0c01160
J. Med. Chem. 2020, 63, 11920−11933

interaction and with MIF-induced ERK phosphorylation and proliferation of A549 cells. Altogether, we identified a novel MIF-binding fluorophore that can be used in competitive binding studies as well as in cell-based assays.

RESULTS

Design and Synthesis. In order to identify a suitable fluorophore for fluorescence quenching binding studies, we set out to investigate a focused compound collection around the 7-hydroxycoumarin scaffold with carbonyl or phenyl substitution in the 3-position. 2,4-Dihydroxybenzaldehyde **1** was employed as the starting material to provide the desired product using the Knoevenagel condensation as a key step as outlined in Scheme 1. Condensation of **1** with diethylmalonate, using piperidine as base, provided **2** in 76% yield. Condensation of **1** with malonic acid afforded intermediate **3** that was converted to compounds **4a** and **4b** by an amidation reaction in yields of 54 and 54%, respectively. *tert*-Butyldimethylsilyl (TBDMS) protection of **1** provided **5** as a starting material for condensation with the corresponding 2-phenylacetic acids to obtain compounds **6a**–**l**. Condensation proceeded with cyanuric chloride and *N*-methylmorpholine (NMM) followed by TBDMS deprotection using TBAF. The yields for these subsequent two reaction steps were 20–90%. All final compounds were purified with chromatography and characterized by ^{1}H and ^{13}C NMR spectroscopy, and LC-HRMS (Supporting Information).

Scheme 1. Synthesis of 7-Hydroxycoumarins as MIF Inhibitors from 2,4-Dihydroxybenzaldehyde 1 as a Key Precursor[a]

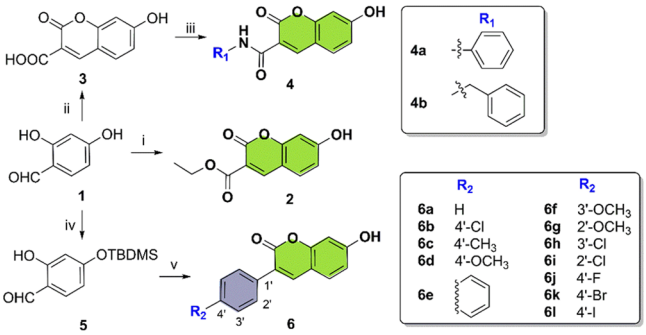

[a]Reagents and conditions: (i) diethyl malonate, piperidine, rt; (ii) malonic acid, pyridine, aniline, rt; (iii) EDCI, HOBt, DMF, rt; (iv) TBDMSCl, imidazole, CH_2Cl_2, rt; (v) (1) cyanuric chloride, NMM, DMF, reflux; (2) TBAF, THF, rt.

SARs. The focused compound collection described above was tested for inhibition of MIF tautomerase activity employing 4-HPP as a substrate as described previously.[35] In brief, the compound stock solution in DMSO was subsequently mixed with aqueous EDTA solution and MIF solution in assay buffer. After 10 min of preincubation, the assay was started by mixing the inhibitor–enzyme mixture with 4-HPP solution. The final reaction mixture contained 225 nM MIF, 0.5 mM 4-HPP, 2.5% (v/v) DMSO, and a variable concentrations of inhibitor. Enzyme activity was monitored by the change in UV absorbance at 306 nm over time. The residual enzyme activity was determined with reference to the positive control for which a corresponding amount of DMSO was used, which was set to 100%. A control reaction in the absence of the enzyme was used as negative control to correct for the spontaneous conversion of the substrate, which was set to 0%. The linear regression parameters were determined to calculate IC_{50} using GraphPad Prism. The IC_{50} values were transformed to K_i values using the Cheng–Prusoff equation: $K_i = IC_{50}/(1 + [S]/K_m)$,[44] in which [S] is the substrate concentration (0.5 mM) and K_m is the Michaelis–Menten constant (1.0 mM).[35]

The SARs for inhibition of the MIF tautomerase activity by the 7-hydroxycoumarins are shown in Table 1. For compound **2**, a K_i of 12.4 ± 1.3 μM was observed, which is in line with a previous report (7.4 ± 2.0 μM).[43] Changing the ester to a substituted amide in compounds **4a** and **4b** decreased the inhibitory potency. In contrast, phenyl substitution at the 7-hydroxycoumarin 3-position in compound **6a** provided 10-fold enhanced potency (K_i of 1.17 ± 0.10 μM) compared to inhibitor **2**. Subsequently, compound **6a** was used as a starting point to evaluate changes in potency upon substitution on the phenyl ring (**6b**–**l**). Substitution of the phenyl *para*-position with a chloro- (**6b**), methyl- (**6c**), methoxyl- (**6d**), fluoro- (**6j**), bromo- (**6k**), or iodo- (**6l**) functionality provided 2- to 3-fold improvement in inhibitory potency. In contrast, replacement of the phenyl with a naphthalene (**6e**) or substitution at the *meta*- or *ortho*-position (**6f**–**i**) did not improve the potency compared to **6a**. Among the *para*-halogen-substituted analogues, bromo-substitution in **6k** provided, with a K_i value of 0.31 ± 0.02 μM, the highest inhibitory potency.

Table 1. Inhibition of the MIF Tautomerase Enzyme Activity by 3-Substituted 7-Hydroxycoumarin Derivatives as Determined by the Conversion of 4-HPP as a Substrate (n = 3, Standard Deviations of the Nonlinear Curve Fitting Are Reported)

	Compound	R	IC_{50} (μM)	K_i (μM)[a]
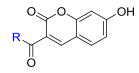	**2**(Orita-1)	-OCH_2CH_3	18.6±1.9	12.4±1.3 [c]
	4a	-NH-C_6H_5	11% [b]	--
	4b	-NH-CH_2-C_6H_5	12% [b]	--
	6a	H	1.76±0.14	1.17±0.10
	6b	4'-Cl	0.92±0.07	0.61±0.05
	6c	4'-CH_3	0.69±0.06	0.46±0.04
	6d	4'-OCH_3	0.56±0.05	0.37±0.03
	6e		2.19±0.30	1.46±0.20
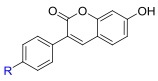	**6f**	3'-OCH_3	1.85±0.14	1.23±0.09
	6g	2'-OCH_3	2.78±0.41	1.85±0.27
	6h	3'-Cl	1.93±0.10	1.29±0.07
	6i	2'-Cl	19.1±3.4	12.7±2.3
	6j	4'-F	2.54±0.27	1.69±0.18
	6k	4'-Br	0.47±0.03	0.31±0.02
	6l	4'-I	0.72±0.06	0.48±0.04

[a]$K_i = IC_{50}/(1 + 0.5/K_m)$. [b]% inhibition at 25 μM. [c]7.4 ± 2.0 μM (Orita-1) in the literature.[43]

Fluorescence Quenching and Indicator-Displacement Assay. From the focused compound collection,

https://dx.doi.org/10.1021/acs.jmedchem.0c01160
J. Med. Chem. 2020, 63, 11920–11933

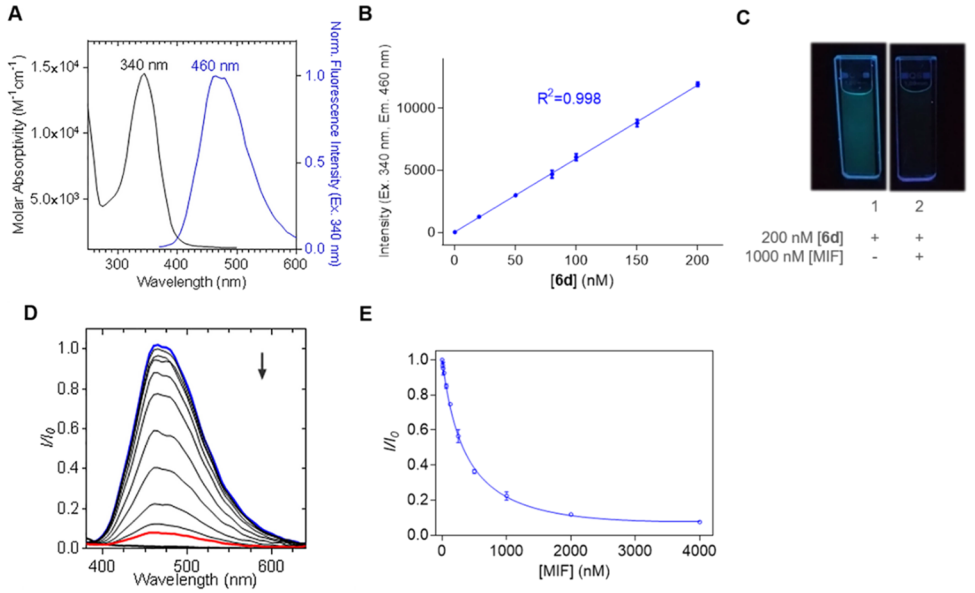

Figure 2. The fluorescence of compound **6d** is quenched upon binding to MIF. (A) UV absorbance (50 μM) and fluorescence emission spectra (200 nM) of **6d**. (B) Concentration–fluorescence intensity correlation of **6d**, n = 3. (C) Fluorescence and fluorescence quenching of **6d** (200 nM) in the absence or presence of MIF (1 μM). (D) Decrease in fluorescence intensity for **6d** (100 nM) with increasing concentration of MIF (10 nM to 4 μM). (E) Concentration-dependent decrease of the fluorescence of **6d** (100 nM) in response to increased concentration of MIF, n = 3. All experiments were conducted in pH 7.4 PBS buffer.

inhibitor **6d** was chosen for the initial exploration of an FID assay for MIF binding. Inhibitor **6d** has a UV absorption maximum at 340 nm in PBS (pH 7.4) and a fluorescence emission maximum at 460 nm, resulting in a Stokes shift of 120 nm (Figure 2A). The fluorescence quantum yield was determined to be 0.25 (Figure S1), which is sufficiently high for the development of a fluorescent sensor for binding studies.[42] Importantly, the fluorescence intensity of **6d** is linearly correlated to its concentration at concentrations below 200 nM (Figure 2B). Fluorescence quenching of **6d** (200 nM) was observed upon addition of MIF (1 μM) (Figure 2C), and the fluorescence quenching is concentration-dependent (Figure 2D). Quantification of the change in fluorescence enabled determination of a dissociation constant of 0.39 ± 0.04 μM for **6d** to MIF (Figure 2E), which is in line with the K_i value calculated from the MIF tautomerase enzyme activity assay. Taken together, this demonstrates that 7-hydroxycoumarin **6d** shows affinity-dependent fluorescence quenching upon binding to the MIF tautomerase active site, which enables quantification of binding.

The affinity-dependent fluorescence quenching of **6d** upon binding to MIF creates chances for development of an FID assay to quantify binding to the MIF tautomerase active site. The quenched fluorescence of **6d** (100 nM) by MIF (1.0 μM) can be recovered by using the nonfluorescent MIF inhibitor **8** in a concentration-dependent manner (Figure 3A). Plotting the fluorescence intensity against the concentration of **8** provided a sigmoidal curve with an effective concentration for a half-recovery of the fluorescence (EC_{50}) of 0.386 ± 0.044 μM as derived by nonlinear curve fitting.

EC_{50} for fluorescence recovery was used to calculate the corresponding K_d value for binding of **8** to MIF by application of eq 1 according to literature procedures.[39,45] In this equation, K_d is the dissociation constant between MIF and the nonfluorescent inhibitor; H_t is the total host (MIF) concentration; I_t is the total concentration of the fluorescent

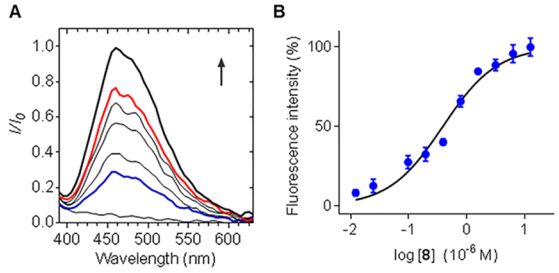

Figure 3. Fluorescence recovery of **6d** in the presence of MIF by **8**. (A) Fluorescence spectra of **6d** (100 nM) together with MIF (1.0 μM) increased with the addition of **8**. (B) Nonlinear regression for log concentration of **8** *vs* response, n = 3.

indicator **6d**; EC_{50} is the concentration of the competitor that provides half-maximal fluorescence recovery; K_S is the dissociation binding constant of the interaction between MIF and fluorescent indicator **6b**; F_b is the fraction of the bound indicator **6b**. Using this equation, a K_d value of 0.156 ± 0.018 μM was calculated for the binding of **8** to MIF. We note that this value corresponds well with a K_i value of 0.100 ± 0.010 μM as determined by the MIF tautomerase activity assay using 4-HPP as a substrate. Binding properties of **8** are also in line with the SARs of a group of structurally similar MIF inhibitors.[37] At this point, we conclude that the FID assay provides a viable alternative for the MIF tautomerase enzyme activity assay used for analysis of MIF binding molecules.

$$K_d = \frac{[(-H_t \times F_b^2) + (K_S + I_t - EC_{50} + H_t) \times F_b + EC_{50} - I_t] \times F_b \times K_S}{(1 - F_b) \times [(I_t \times F_b^2) - ((K_S + I_t + H_t) \times F_b) + H_t]} \quad (1)$$

Assay Optimization. In the next step, we set out to improve the FID assay by development of a 7-hydroxycoumarin with a higher affinity for MIF to gain sensitivity and enable reduction of the concentrations of both the fluorophore and

https://dx.doi.org/10.1021/acs.jmedchem.0c01160
J. Med. Chem. 2020, 63, 11920−11933

MIF. Improved affinity was achieved by expansion of the substituent on the *para*-position of the 3-phenyl-7-hydroxycoumarin scaffold with a 4′-carboxyphenyl functionality. This functionality was installed using a Suzuki cross-coupling reaction on the *para*-iodophenyl derivative **6l** to provide 7-hydroxycoumarin **7** (Scheme 2). Interestingly, **7** exhibited a

Scheme 2. Synthesis of 7[a]

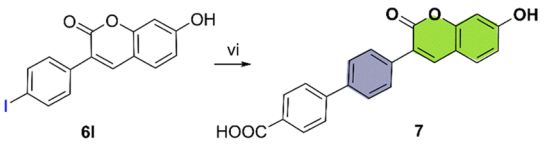

[a]Reagents and conditions: (vi) 4-boronobenzoic acid, $Pd(AcO)_2$, Na_2CO_3, EtOH, rt.

10-fold increased potency compared to its precursor **6l** in the MIF tautomerase activity assay to provide an IC_{50} value of 71 ± 3 nM, which indicates tight-binding properties. Because of the tight-binding properties, the Morrison equation was used to calculate the binding constant of **7**, which proved to be 16 ± 1 nM (see Figure S2).[46]

To rationalize binding of **7** to MIF, a docking study was performed for compound **7** using the crystal structure of MIF bound to inhibitor **2** (Orita-1) (PDB code: 1GCZ).[43] Inhibitor **2** (Orita-1) was removed from the binding site and redocked to validate the docking protocol. The 7-hydroxylcoumarin part of **2** (Orita-1) occupies the active site that harbors the MIF tautomerase activity. There is a second hydrophobic region at the rim of the tautomerase active site to which **2** (Orita-1) does not bind. The highest-scoring docking poses for compound **7** can occupy the same position as observed for **2** (Orita-1) to provide similar interactions of the coumarin core (Figure 4A and Figure S8). The major difference between **2**

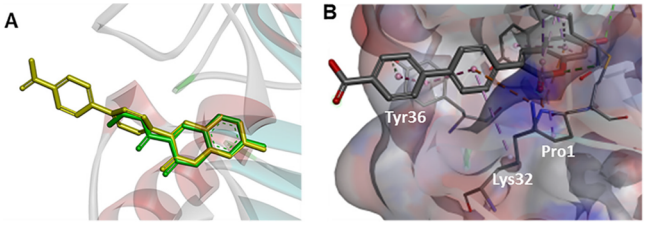

Figure 4. Molecular modeling of compound **7** in the MIF tautomerase active site (PDB code: 1GCZ).[43] (A) Overlay for binding of **2** (Orita-1) (green) and **7** (yellow) to the MIF tautomerase active site. The protein is shown in ribbon diagram. Inhibitors are displayed as sticks. (B) Binding of **7** to the MIF tautomerase active site shown in surface representation. The interactions between phenyl rings of **7** and rim residues Tyr36 and Lys32 are highlighted.

(Orita-1) and **7** resides in the substitution at the coumarin 3-position. **2** (Orita-1) formed a hydrophobic interaction between the ethyl group of the ester and Lys32. In contrast, for compound **7**, both phenyl rings at the coumarin 3-position formed $\pi-\pi$ stacking interactions with Tyr36 and hydrophobic interactions with Pro1 and Lys32 (Figure 4B) at the rim of the tautomerase active site. Thus, compound **7** provides additional interactions with the hydrophobic rim of the MIF tautomerase active site, which explains the higher MIF binding potency observed for inhibitor **7**.

Meanwhile, **7** also demonstrated favorable fluorescence properties with a quantum yield of 0.32, a Stokes shift of 100 nm (Figure 5A), and concentration-dependent fluorescence quenching upon binding to MIF in (Figure 5B). Using this fluorescence quenching experiment, the binding constant K_S of **7** was determined to be 16 ± 3 nM (Figure 5C), which is again in line with the inhibition of the MIF tautomerase activity (K_i = 18 ± 1 nM). The high affinity of **7** for MIF enabled the reduction of both the fluorophore (50 nM) and MIF (100 nM) concentrations in the FID assay. This provides an assay format that is sufficiently sensitive to quantify the binding affinity of MIF ligands with nanomolar potencies.

The FID assay was established with fluorophore **7**. First, a control experiment for non-MIF-dependent fluorescence quenching was performed with a corresponding amount of bovine serum albumin (BSA). In clear contrast to MIF, no fluorescence quenching was observed upon the addition of 800 nM BSA to a 50 nM solution of fluorophore **7** (Figure 5C). Enzyme kinetics experiments demonstrated that **7** binds in competition with 4-HPP (Figure 5D). As a next step, we aimed to distinguish static *versus* dynamic fluorescence quenching by determination of the fluorescence lifetime of **7** (100 nM) in the absence (τ_0) or in the presence (τ) of MIF (500 nM), which proved to be 4.2 and 4.0 ns, respectively (Figure 5E). The constant value for the fluorescence lifetime demonstrates that fluorescence quenching is static, which implies that quenching occurs by specific binding of the fluorophore to a cavity in the protein rather than by random collision-induced energy transfer. In addition, the influence of the solvent on the fluorescence intensity of **7** (200 nM) was investigated. The fluorescence proved to be the strongest in PBS buffer (Figure 5F), which indicates that an aqueous environment is most suitable for this fluorophore. The steep decrease in fluorescence in hydrophobic solvents, such as THF and toluene, indicates that hydrophobicity of the binding site of MIF could play a role in fluorescence quenching upon binding.

We previously observed that the MIF tautomerase activity assay using 4-HPP as a substrate was sensitive to the presence of heavy metal ions such as Cu^{2+}.[35] Therefore, the influence of Cu^{2+} ions on this FID assay for MIF binding using **7** as a fluorophore was investigated. Importantly, no influence of Cu^{2+} ions was observed up to a concentration of 200 μM (Figure S5), which indicates that this assay format is not sensitive to interference by this heavy metal ion.

Thus, the FID assay using fluorescent indicator **7** was established as a method for competition-based binding studies to the MIF tautomerase active site. This assay was used to determine the affinities of a series of structurally diverse MIF tautomerase inhibitors (Figure 6)[35,47] for validation. This assay was performed in a 96-well format in which each well contained 100 μL of MIF (200 nM, in pH 7.4 PBS buffer) and 50 μL of inhibitor in various concentrations in PBS (pH 7.4 with 10% (v/v) DMSO). The mixture was incubated for 10 min at room temperature, and subsequently, 50 μL of indicator **7** (200 nM) in PBS buffer (pH 7.4) was added and incubated for 10 min before the fluorescence intensity was recorded at Ex/Em = 355/455 nm. The window coefficient (*Z*′-factor) of this assay was evaluated for an inhibition curve of **8** and proved to be 0.75 in this setup (SI 6), which indicates that the quality of this assay is sufficient for medium- to high-throughput applications (0.5−1).[48] Using the FID assay, the EC_{50} values for the structurally diverse series of MIF tautomerase inhibitors were determined and used to calculate the K_d values using eq

https://dx.doi.org/10.1021/acs.jmedchem.0c01160
J. Med. Chem. 2020, 63, 11920−11933

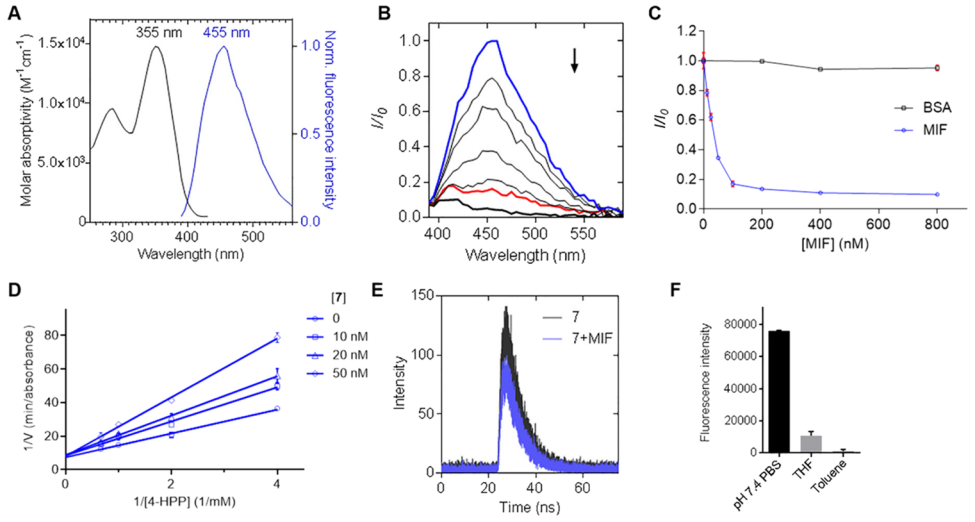

Figure 5. Fluorescence properties of 7 and its fluorescence quenching upon MIF binding. (A) UV absorbance and fluorescence emission spectra of 7. (B) Fluorescence quenching of 50 nM 7 by MIF (12.5−200 nM). (C) Quantification of fluorescence quenching of 50 nM 7 by MIF or BSA. (D) Lineweaver−Burk plot of inhibition of 7 against MIF tautomerase. (E) Fluorescence lifetime study in 1 mL of pH 7.4 PBS; half-life of 100 nM fluorophore is 4.2 ns and together with 500 nM MIF is 4.0 ns. (F) Fluorescence intensity of 200 nM 7 in different solvents, Ex/Em = 355/455 nm.

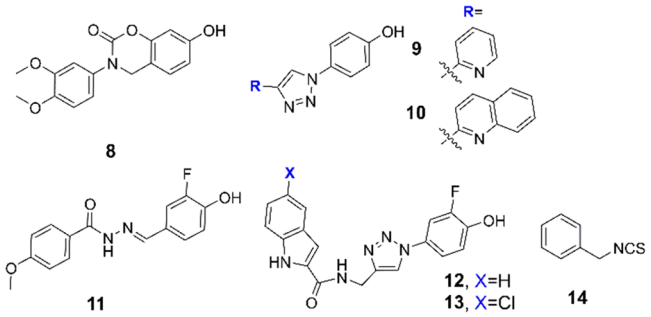

Figure 6. Structurally diverse MIF inhibitors that were used to compare the MIF tautomerase enzyme activity assay to the FID assay. Compound **8** is an analogue of NVS-2;[37] **9** and **10** are two typical biaryltrizoles synthesized by the Jorgensen lab;[47] **11** is a phenolic hydrazone analogue;[49] **12** and **13** were reported by our lab.[35] **14** (benzyl isothiocyanate, BITC) is a covalent inhibitor of MIF.[50,51]

Table 2. Results for MIF Tautomerase Activity Inhibition (K_i) from the 4-HPP Conversion Assay and for MIF Binding (K_d) from the Fluorescent Indicator Displacement Assay Using Compound 7 as a Probe[a]

compound	K_i (μM)	K_d (μM)
ISO-1	44 ± 4.9	47 ± 6.3
8	0.10 ± 0.01	0.11 ± 0.01
9	5.0 ± 0.6	4.0 ± 0.5
10	0.44 ± 0.03	0.47 ± 0.08
11	8.0 ± 0.6	5.6 ± 0.5
12	3.3 ± 0.6	4.4 ± 0.3[b]
13	0.96 ± 0.2	1.4 ± 0.1
14[c]	4.3 ± 0.3	2.9 ± 0.4

[a]Data are shown as mean ± SD of three independent experiments. [b]The K_d value measured by microscale thermophoresis (MST) was 3.6 μM.[35] [c]Measured after 10 min of incubation.

1. Comparison of the K_d values as determined by the FID assay to the K_i values as calculated from the MIF tautomerase enzyme activity assay indicated that both methods provide comparable affinity values (Table 2), thus indicating that the FID assay is a reliable and accurate alternative for the MIF tautomerase enzyme activity assay.

Inhibition of the MIF−CD74 PPI. The high affinity of 7 for the MIF tautomerase active site raised the question if this compound also interferes with the MIF−CD74 PPI. To address this question, a previously published ELISA assay to monitor the interaction between MIF and sCD74 was used.[52] In this assay, human recombinant MIF was coated on a 96-well ELISA plate by incubation at 4 °C overnight. After removal of the unbound MIF and blocking with 2% (w/v) BSA, the plate was incubated with a mixture of MBP−sCD74 (500 nM) and inhibitor for half an hour. Subsequently, bound MBP−sCD74 was detected using an anti-CD74 primary antibody and a signal amplifying secondary antibody. The signal for MBP−sCD74 in the absence of the inhibitor was set to 100%, and the signal in which MBP−sCD74 was replaced by blank PBS buffer was used as a negative control and set to 0%. Compound 7 provided a dose-dependent inhibition of the sCD74 binding to MIF with an IC_{50} of 36 ± 3 μM (Figure 7). The MIF tautomerase inhibitors ISO-1 and compound **8** were subjected to the same assay but did not demonstrate inhibition at concentrations up to 50 μM (Figure S8). Thus, compound 7 interferes with the MIF−sCD74 interaction in this assay format.

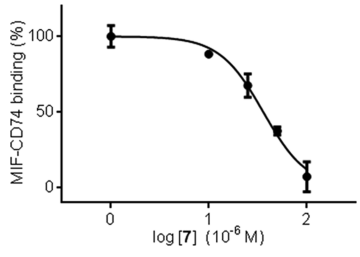

Figure 7. Compound 7 inhibits the MIF−sCD74 binding as determined by an ELISA assay. Binding of MBP−sCD74 to MIF-coated ELISA plates was detected using a rabbit anti-CD74 antibody as the primary and a goat anti-rabbit horseradish peroxidase conjugate as the secondary antibody. Data are displayed as mean ± SD (n = 3).

https://dx.doi.org/10.1021/acs.jmedchem.0c01160
J. Med. Chem. 2020, 63, 11920−11933

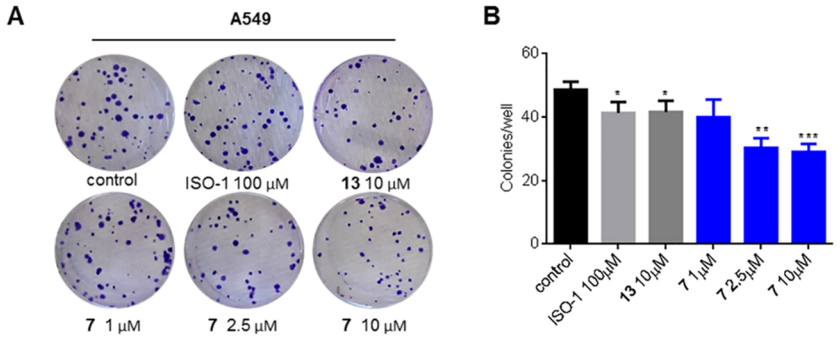

Figure 8. Inhibition of cell proliferation by MIF inhibitors. (A) Representative pictures of clonogenic assays. A549 cells (100 cells per well) were treated with appropriate inhibitors and stained with crystal violet. (B) Colony quantification provided a bar graph showing inhibition of colony formation upon treatment with MIF inhibitors ISO-1, **13**, or **7**. Colonies were counted by ImageJ and confirmed by manual counting. One colony was estimated as an aggregate of >50 cells. Data are shown as mean ± SD of three independent experiments. *$p < 0.05$, **$p < 0.01$, and ***$p < 0.001$ *vs* control group.

Cell-Based Study. MIF-induced signaling proceeds through binding to the CD74 receptor, activation of the MAPK signaling pathway, and can result in cell proliferation.[6] The ability of inhibitor **7** to interfere with MIF-induced signaling was investigated in A549 cells.[53] As a first step, an MTS assay was performed, which demonstrated that compound **7** did not inhibit cell viability at concentrations below 20 μM upon 24 h of treatment (Figure S9). Next, the growth inhibitory potency of compound **7** in A549 was studied by a colony-forming assay. Compounds ISO-1 and **13** were used as references to a prior literature,[35] and they inhibited colony formation at 100 and 10 μM, respectively (Figure 8). Treatment with inhibitor **7** in doses of 2.5 or 10 μM resulted in significantly lower numbers of colonies. These data demonstrate that **7** is a more potent inhibitor of A549 cell proliferation than ISO-1 and **13**.

As a next step, the influence of **7** on MIF-induced ERK phosphorylation was investigated in A549 cells. Toward this aim, A549 cells were stimulated with MIF or compound **7** preincubated MIF, and subsequently, ERK phosphorylation was detected by Western blot. We found that compound **7** attenuated MIF-induced ERK phosphorylation in A549 cells (Figure 9) at a concentration of 10 μM.

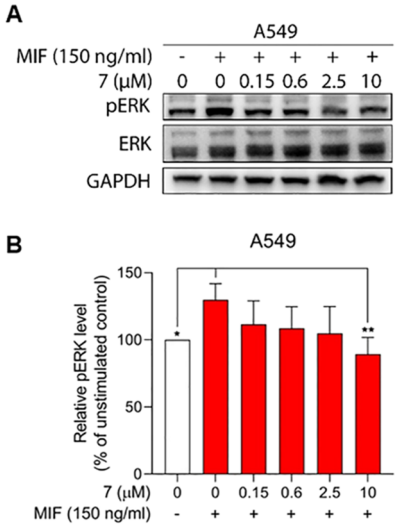

Figure 9. Effect of MIF inhibitor **7** on MIF-induced ERK phosphorylation in A549 cells. (A) A representative result of the Western blot experiment. 150 ng/mL MIF was incubated with or without appropriate concentrations of MIF inhibitors for 10 min followed by stimulation at 37 °C for 10 min. (B) Quantification of the pERK level using the pERK/GAPDH ratio. In the control group, vehicle was applied without MIF. In the vehicle group, MIF was incubated with an appropriate amount of DMSO. Data are shown as mean ± SD of four independent experiments. *$p < 0.05$ and **$p < 0.01$ *vs* vehicle group.

DISCUSSION AND CONCLUSIONS

In this study, we set out to develop an FID assay for competitive binding studies on the MIF tautomerase active site. Toward this aim, we employed 7-hydroxycoumarins as fluorophores that quench fluorescence upon binding to the tautomerase active site.[42,43] In order to identify 7-hydroxycoumarins with high potency, a focused collection of 3-substituted 7-hydroxycoumarins were synthesized and inhibition of MIF tautomerase enzyme activity was investigated. We observed that compounds with a phenyl substituent in the 7-hydroxycoumarin 3-position were more potent than derivatives with an ester or amide functionality in this position. This result is in line with the literature in which the hydrophobic surface at the rim of active site of MIF was described to be involved in the enhanced potency of 3-phenyl-substituted 7-hydroxycoumarins.[43] Further analysis of the SARs indicated that *para*-phenyl substitutions in the 3-position of 7-hydroxycoumarins that add bulk and are weakly electron-withdrawing are favorable for the potency of inhibitors. This inspired the design of an inhibitor with a *para*-benzoic acid functionality. Inhibitor **7** proved to be the most potent inhibitor of this series with a K_i of 18 ± 1 nM. This confirms that MIF tautomerase inhibitors that bind both in the active site to residues such as Asn97 and Tyr95 and on the hydrophobic edge of the active site to residue Tyr36 provide low-nanomolar potency.[43] Taken together, we obtained one of the most potent MIF tautomerase inhibitors by exploiting the interactions with both the MIF tautomerase active site and the rim of the active site.

7-Hydroxy- and 7-aminocoumarins are widely used fluorescent sensors in biological applications.[42] Therefore, the fluorescence properties of the 7-hydroxycoumarin MIF inhibitors were exploited for the development of an FID assay for binding to the MIF tautomerase active site. The fluorogenic properties of MIF inhibitors **6d** and **7** are favorable with a Stokes shift exceeding 100 nm and quantum yields of 0.25 and 0.32, respectively. Importantly, the fluorescence of both **6d** and **7** quenched upon MIF addition in a

https://dx.doi.org/10.1021/acs.jmedchem.0c01160
J. Med. Chem. 2020, 63, 11920−11933

Table 3. Potency, *C* log *P*, Solubility, and Ligand Efficiency Values of MIF Tautomerase Inhibitors

compound	K_i (μM)	MW	*C* log *P*[a]	solubility (μg/mL)	LE[b]	LLE[c]
ISO-1	44 ± 4.9	235.08	1.69		0.34	2.48
7	0.018 ± 0.001	357.08	1.35	18.8 ± 1.4	0.37	5.80
8	0.10 ± 0.01	302.10	1.97		0.43	4.85
10	0.44 ± 0.03	385.07	3.64	2.2[47]	0.39	2.55
13	0.96 ± 0.2	288.10	3.80	10.8 ± 0.10[35]	0.30	2.05

[a]Calculated by ChemDraw Professional 18.1. [b]LE (ligand efficiency) =1.4(−log IC_{50})/*N*, where *N* is the number of non-hydrogen atoms. [c]LLE (lipophilic ligand efficiency) = pIC_{50} − *C* log *P*, pIC_{50} = −log IC_{50}.

concentration-dependent manner. Binding of the 7-hydroxycoumarin fluorophores to the MIF tautomerase active site proved to be reversible, which enabled development of a competitive binding assay to recover the 7-hydroxycoumarin fluorescence. Using fluorescence lifetime analysis, we found fluorescence quenching of **7** upon binding to MIF to be static rather than dynamic. This excludes fluorescence quenching by random collision, which also qualifies **7** as an appropriate fluorophore for FID assay development. Therefore, **7** was used as the most potent MIF binder with suitable fluorogenic properties for the development of an FID assay to quantify binding to the MIF tautomerase active site. This assay employs the same format as applied for other targets such as carbonic anhydrase and retinoid X receptor.[40,54] Most fluorescent indicators contain three parts: a specific high-affinity target binding moiety, a linker, and a fluorophore. In contrast, 7-hydroxycoumarin **7** is a fluorophore and a high-affinity binder at the same time. Furthermore, **7** is a small molecule that can be synthesized in only four steps including TBDMS protection and deprotection, which makes this molecule and assay format easily accessible.

The FID assay using **7** as a fluorophore was validated through measuring binding affinities of a group of structurally diverse MIF tautomerase inhibitors. The consistency between K_d values assessed by the FID assay and the K_i values measured by the enzymatic tautomerase assay (Table 2) demonstrates that the FID assay is a reliable substitution for the MIF tautomerase assay. Notably, the FID assay has several advantages. For example, in contrast to the 4-HPP tautomerase assay, the FID assay can be performed in PBS buffer and does not require reduced pH and borate buffer (Figure S10). The presence of metal ions such as Cu^{2+} did not interfere with the FID assay in contrast to the tautomerase activity assay, which reduces the chance for irregularities in the assay.[35] In addition, the FID assay employs 100 nM MIF, which is more sensitive than the MIF tautomerase assay that typically requires 200−400 nM MIF.[47] We note that the FID assay could provide false positive results by fluorescence quenching through the competing ligand, for which proper controls need to be included. We also note that K_i values of reference compounds measured by the 4-HPP tautomerase assay are consistent among different labs[43,47] and also in line with K_d values measured by other assays,[35,37] which demonstrates that the MIF tautomerase assay itself is also a reliable assay if handled properly. Irregularities as reported previously in the literature[36] can be excluded by proper operation of the respective assay. We envision that the FID assay will gain a role as a complementary assay to the 4-HPP tautomerase assay.

Besides its use as a fluorescent indicator for MIF binding, compound **7** was also analyzed for its ability to interfere with MIF-induced signaling. The CD74 receptor is important for MIF-induced signaling and can mediate the MIF-induced cell growth and proliferation.[6,9] Interestingly, compound **7** interfered with the MIF−sCD74 interactions in an ELISA assay. This implies that molecules that bind to the MIF tautomerase active site also interfere with the MIF−CD74 PPI, in line with the literature.[24] We anticipate that interference with the MIF−CD74 PPI is enabled by interactions between compound **7** with Tyr36 of MIF, which is a key residue for the PPI.[24] However, we also note that a significant "drop-off" in potency is observed for inhibition of the MIF−CD74 interaction in comparison to MIF binding. Similar inconsistencies were reported in an earlier literature.[55] We have the impression that the MIF−CD74 interaction has some unresolved issues with respect to binding stoichiometry in connection to binding avidity. The ELISA assay format, as applied here, might influence the binding avidity of the MIF−CD74 interaction, which influences inhibitor binding potency. Nevertheless, inhibitor **7** also inhibited MIF-induced ERK phosphorylation and colony formation of A549 cells in the clonogenic assay. Taken together, our results provide further evidence that MIF-induced signaling can be inhibited by small-molecule inhibitors that target the MIF tautomerase active site.[28]

The currently available inhibitors of MIF tautomerase activity suffer often from poor physicochemical properties such as poor water solubility and high *C* log *P* values, which can, among others, result in irregularities in the assay readout.[36] Notably, the solubility of compound **7** in pH 7.4 PBS buffer was 18.8 ± 1.4 μg/mL (53 ± 3.9 μM), which overcomes the solubility issue of the triazole inhibitors.[47] Furthermore, ligand efficiency and lipophilic ligand efficiency of **7** are calculated to be 0.37 and 5.80, respectively, which are favorable for biological activity (>0.3 for LE, and >5.0 for LLE).[56] This demonstrates that inhibitor **7** has favorable physicochemical properties and good efficiency and potency against MIF tautomerase activity (Table 3) as well as in cell-based assays on MIF-induced signaling.

In conclusion, we have developed a convenient and effective FID assay to evaluate the affinity of MIF tautomerase active site binders. The fluorescent indicator **7** was designed based on the SARs of a group of 7-hydroxylcoumarin derivatives. **7** displays clear fluorescence quenching upon binding to the MIF tautomerase active site that is reversible in the presence of competing ligands. Using fluorophore **7**, an FID assay was developed that enabled quantification of MIF binding in a competition assay. This assay system proved to be more sensitive than the 4-HPP tautomerase assay and can be performed in neutral pH in PBS buffer. These results demonstrate that **7** is a convenient fluorescent probe for MIF binding studies in an FID assay format. The most potent MIF enzyme inhibitor **7** provides inhibition of the MIF−CD74 PPI and interferes with MIF-induced ERK phosphorylation as well as cell growth in a clonogenic assay with A549 cancer cells

https://dx.doi.org/10.1021/acs.jmedchem.0c01160
J. Med. Chem. 2020, 63, 11920−11933

at micromolar concentrations. Taken together, compound 7 provides a valuable novel tool to advance MIF-oriented research.

EXPERIMENTAL SECTION

General. All the reagents and solvents were purchased from Sigma-Aldrich, TCI, Fluorochem, or Acros and were used without further purification. Reactions were monitored by thin layer chromatography (TLC), in which Merck silica gel 60 F_{254} plates were used and spots were detected with UV light. MP Ecochrom silica 32−63, 60 Å was used for column chromatography. Nuclear magnetic resonance spectra, ^{1}H NMR (500 MHz) and ^{13}C NMR (126 MHz), were recorded on a Bruker Avance 500 spectrometer. Chemical shifts were reported in ppm. Chemical shifts were referenced to the residual proton and carbon signals of the deuterated solvent, $CDCl_3$: δ = 7.26 (^{1}H) and 77.05 ppm (^{13}C) or DMSO-d_6: δ = 2.50 (^{1}H) and 39.52 ppm (^{13}C). The following abbreviations were used for spin multiplicity: s (singlet), d (doublet), t (triplet), q (quartet), dd (double of doublets), and m (multiplet). Coupling constants were reported in hertz (Hz). High-resolution mass spectra were recorded using Fourier transform mass spectrometry (FTMS) and electrospray ionization (ESI) on an Applied Biosystems/SCIEX API3000-triple quadrupole mass spectrometer. Purity of the compounds was determined by reversed-phase high-performance liquid chromatography (HPLC) analysis to be >95%.

Ethyl 7-Hydroxy-2-oxo-2*H*-chromene-3-carboxylate (2).[57] 2,4-Dihydroxybenzaldehyde (569 mg, 4.12 mmol) was dissolved in diethyl malonate (1.5 mL) and piperidine (0.5 mL). The mixture was stirred at room temperature overnight. The resulting solution was acidified with an aqueous solution of HCl (1 N, 5 mL). The precipitate was filtered and washed with cold water (10 mL × 2). 850 mg of desired product was obtained as a yellow solid. Purity was 97% determined by HPLC. Yield 76%. ^{1}H NMR (500 MHz, DMSO-d_6) δ 11.11 (s, 1H), 8.68 (s, 1H), 7.76 (d, J = 8.6 Hz, 1H), 6.85 (dd, J = 8.6, 2.2 Hz, 1H), 6.74 (d, J = 2.1 Hz, 1H), 4.26 (q, J = 7.1 Hz, 2H), 1.30 (t, J = 7.1 Hz, 3H). ^{13}C NMR (126 MHz, DMSO) δ 164.5, 163.4, 157.6, 156.9, 149.93, 132.6, 114.46, 112.5, 110.9, 102.3, 61.3, 14.6. HRMS, calculated for $C_{12}H_{11}O_5$ $[M + H]^+$: 235.0601, found 235.0598.

7-Hydroxy-2-oxo-2*H*-chromene-3-carboxylic Acid (3).[58] Malonic acid (1.35 g, 13 mmol) was dissolved in pyridine (4 mL) followed by addition of 2,4-dihydroxybenzaldehyde (1.0 g, 7.3 mmol) and aniline (0.1 mL). After stirring at room temperature overnight, the mixture was acidified with 1 N HCl to pH 4.0. The precipitate was isolated by filtration and recrystallization in methanol to provide 1.3 g of product as a yellow solid, yield 89%, R_f value 0.60 (CH_2Cl_2/MeOH, 10:1). ^{1}H NMR (500 MHz, DMSO-d_6) δ 12.89 (s, 1H), 11.07 (s, 1H), 8.68 (s, 1H), 7.75 (d, J = 8.6 Hz, 1H), 6.84 (dd, J = 8.6, 2.2 Hz, 1H), 6.74 (d, J = 2.2 Hz, 1H). ^{13}C NMR (126 MHz, DMSO) δ 164.7, 164.4, 158.00, 157.5, 149.9, 132.5, 114.5, 113.0, 111.1, 102.3.

7-Hydroxy-2-oxo-*N*-phenyl-2*H*-chromene-3-carboxamide (4a). 3 (80 mg, 0.4 mmol) was mixed with aniline (60 μL) in dry DMF (2 mL) followed by adding EDCI (120 mg, 0.8 mmol) and HOBt (70 mg, 0.5 mmol). The yellow solution was stirred under an argon atmosphere at room temperature overnight. Subsequently, the reaction mixture was diluted with CH_2Cl_2 (20 mL) and washed with a saturated aqueous NaCl solution (20 mL). The organic layer was concentrated under reduced pressure to obtain the crude product, which was purified by column chromatography using CH_2Cl_2 as the eluent. 80 mg of pale yellow powder was obtained with a yield of 54%, R_f value 0.30 (CH_2Cl_2/MeOH, 20:1). ^{1}H NMR (500 MHz, DMSO-d_6) δ 11.15 (s, 1H), 10.65 (s, 1H), 8.87 (s, 1H), 7.86 (d, J = 8.6 Hz, 1H), 7.71 (d, J = 7.9 Hz, 2H), 7.37 (t, J = 7.8 Hz, 2H), 7.13 (t, J = 7.4 Hz, 1H), 6.91 (dd, J = 8.6, 2.1 Hz, 1H), 6.84 (d, J = 2.0 Hz, 1H). ^{13}C NMR (126 MHz, DMSO) δ 164.4, 161.8, 160.6, 156.9, 148.88, 138.5, 132.69, 129.5, 124.6, 120.3, 115.0, 114.6, 111.7, 102.4. HRMS, calculated for $C_{16}H_{12}O_4N$ $[M + H]^+$: 282.0761, found 282.0757.

***N*-Benzyl-7-hydroxy-2-oxo-2*H*-chromene-3-carboxamide (4b).** 3 (70 mg, 0.3 mmol) was mixed with benzylamine (100 μL, 1.0 mmol) in dry DMF (1 mL) followed by addition of EDCI (120 mg, 0.8 mmol) and HOBt (70 mg, 0.5 mmol). The yellow solution formed was stirred at room temperature with argon for overnight. Afterward, the reaction mixture was diluted with CH_2Cl_2 (10 mL) and washed with water (10 mL × 2). The aqueous layer was washed with CH_2Cl_2 (10 mL × 3). The organic layer was collected and dried with $MgSO_4$, filtered, and concentrated by reduced pressure evaporation. The product was purified by chromatography with petroleum ether and ethyl acetate 1:1. 80 mg of white solid was obtained with a yield of 54%, R_f value 0.40 (CH_2Cl_2/MeOH, 20:1). ^{1}H NMR (500 MHz, DMSO-d_6) δ 11.06 (s, 1H), 9.05 (t, J = 6.0 Hz, 1H), 8.81 (s, 1H), 7.82 (d, J = 8.7 Hz, 1H), 7.33 (m, 4H), 7.25 (m, 1H), 6.88 (dd, J = 8.6, 2.2 Hz, 1H), 6.80 (d, J = 2.0 Hz, 1H), 4.53 (d, J = 6.0 Hz, 2H). ^{13}C NMR (126 MHz, DMSO) δ 164.1, 162.2, 161.5, 156.8, 148.7, 139.6, 132.5, 128.9, 127.8, 127.4, 114.8, 114.2, 111.6, 102.3, 43.1. HRMS, calculated for $C_{16}H_{12}O_4N$ $[M + H]^+$: 296.0917, found 296.0917.

4-((*tert*-Butyldimethylsilyl)oxy)-2-hydroxybenzaldehyde (5). 2,4-Dihydroxybenzaldehyde (0.40 g, 2.9 mmol) and imidazole (0.22 g, 3.2 mmol) were dissolved in CH_2Cl_2 (6 mL) followed by portionwise addition of *tert*-butyldimethylsilyl chloride (TBDMS-Cl) (0.44 g, 2.9 mmol). The mixture was stirred at room temperature for 1.5 h, and progress of the reaction was monitored by TLC analysis. Upon disappearance of the starting material, CH_2Cl_2 (10 mL) was added to dilute the mixture. The organic layer was subsequently washed with water (20 mL × 3) and brine (20 mL) and dried over $MgSO_4$. After filtering $MgSO_4$, organic solvent was removed under reduced pressure by a rotary evaporator. The product was obtained as a clear oily liquid, which was used without further purification in the next step. ^{1}H NMR (500 MHz, chloroform-d) δ 11.36 (s, 1H), 9.75 (s, 1H), 7.43 (d, J = 8.5 Hz, 1H), 6.50 (dd, J = 8.5, 2.2 Hz, 1H), 6.41 (d, J = 2.2 Hz, 1H), 1.01 (s, 9H), 0.28 (s, 6H).

General Procedure for the Synthesis of Compounds 6a−l (Using 6a as an Example).[59] 2-Phenylacetic acid (136 mg, 1.0 mmol) and cyanuric chloride (190 mg, 1.0 mmol) were dissolved in anhydrous DMF (2 mL). *N*-Methyl morpholine (160 μL, 1.5 mmol) was added into the flask, and the mixture was stirred at room temperature for 10 min. 4-((*tert*-Butyldimethylsilyl)oxy)-2-hydroxybenzaldehyde (250 mg, 1.0 mmol) was dissolved in DMF (1 mL) and added dropwise to the reaction mixture. The resulting suspension was refluxed under argon overnight. The reaction was monitored using TLC, and the coumarin product showed strong fluorescence under UV light (365 nm). The reaction was stopped by addition of demineralized water (15 mL). The mixture was extracted with ethyl acetate (15 mL × 3). The organic phase was collected, washed with brine, dried over $MgSO_4$, and filtered, and the solution was concentrated under reduced pressure by a rotary evaporator. The residue was dissolved in THF (4 mL), and tetra-*n*-butylammonium fluoride (TBAF) (260 mg, 1.0 mmol) was added. The suspension was stirred at room temperature for 1 h. The reaction mixture was diluted with CH_2Cl_2 (20 mL), and the organic phase was washed with brine (20 mL × 3), dried over $MgSO_4$, filtered, and concentrated under reduced pressure. The product was purified by column chromatography using CH_2Cl_2/MeOH (100:1) as the eluent followed by recrystallization from MeOH to provide the pure product as a pale yellow powder in an overall yield of 55%.

*7-Hydroxy-3-phenyl-2H-chromen-2-one (**6a**).* Pale yellow solid, yield 55%, R_f value 0.35 (CH_2Cl_2/MeOH, 20:1). ^{1}H NMR (500 MHz, DMSO-d_6) δ 10.65 (s, 1H), 8.16 (s, 1H), 7.69 (d, J = 7.2 Hz, 2H), 7.60 (d, J = 8.5 Hz, 1H), 7.44 (t, J = 7.5 Hz, 2H), 7.38 (t, J = 7.3 Hz, 1H), 6.82 (dd, J = 8.5, 2.3 Hz, 1H), 6.76 (d, J = 2.3 Hz, 1H). ^{13}C NMR (126 MHz, DMSO) δ 161.3, 160.1, 154.9, 141.2, 135.1, 130.0, 128.3, 128.20, 128.0, 122.2, 113.4, 112.0, 101.7. HRMS, calculated for $C_{15}H_{11}O_3$ $[M + H]^+$: 239.0708, found 239.0701.

*3-(4-Chlorophenyl)-7-hydroxy-2H-chromen-2-one (**6b**).* Pale yellow solid, yield 62%, R_f value 0.30 (CH_2Cl_2/MeOH, 20:1). ^{1}H NMR (500 MHz, DMSO-d_6) δ 10.66 (s, 1H), 8.21 (s, 1H), 7.74 (d, J = 8.6 Hz, 2H), 7.61 (d, J = 8.5 Hz, 1H), 7.50 (d, J = 8.6 Hz, 2H), 6.83 (dd, J = 8.5, 2.3 Hz, 1H), 6.76 (d, J = 2.2 Hz, 1H). ^{13}C NMR (126 MHz, DMSO) δ 161.5, 159.9, 155.0, 141.4, 133.9, 132.7, 130.2, 130.0,

https://dx.doi.org/10.1021/acs.jmedchem.0c01160
J. Med. Chem. 2020, 63, 11920−11933

128.2, 120.8, 113.5, 111.9, 101.8. HRMS, calculated for $C_{15}H_{10}O_3Cl$ $[M + H]^+$: 273.0313, found 273.0309.

*7-Hydroxy-3-(p-tolyl)-2H-chromen-2-one (**6c**).* Pale yellow solid, yield 50%, R_f value 0.30 (CH_2Cl_2/MeOH, 20:1). ^1H NMR (500 MHz, DMSO-d_6) δ 10.58 (s, 1H), 8.12 (s, 1H), 7.59 (m, 3H), 7.24 (d, J = 7.8 Hz, 2H), 6.82 (dd, J = 8.4 Hz, 2.3 Hz, 1H), 6.75 (d, J = 2.2 Hz, 1H), 2.34 (s, 3H). ^{13}C NMR (126 MHz, DMSO) δ 161.1, 160.1, 154.8, 140.5, 137.4, 132.2, 129.9, 128.8, 128.1, 122.1, 113.3, 112.1, 101.7, 20.8. HRMS, calculated for $C_{16}H_{13}O_3$ $[M + H]^+$: 253.0859, found 253.0855.

*7-Hydroxy-3-(4-methoxyphenyl)-2H-chromen-2-one (**6d**).* Pale yellow solid, yield 37%, R_f value 0.30 (CH_2Cl_2/MeOH, 20:1). ^1H NMR (500 MHz, DMSO-d_6) δ 10.57 (s, 1H), 8.10 (s, 1H), 7.66 (d, J = 8.8 Hz, 2H), 7.59 (d, J = 8.5 Hz, 1H), 7.01 (d, J = 8.8 Hz, 2H), 6.82 (dd, J = 8.5, 2.2 Hz, 1H), 6.75 (d, J = 2.0 Hz, 1H), 3.80 (s, 3H). ^{13}C NMR (126 MHz, DMSO) δ 161.4, 160.7, 159.6, 155.1, 140.2, 130.2, 130.0, 127.8, 122.3, 114.1, 113.8, 112.6, 102.1, 55.7. HRMS, calculated for $C_{16}H_{13}O_4$ $[M + H]^+$: 269.0814, found 269.0804.

*7-Hydroxy-3-(naphthalen-2-yl)-2H-chromen-2-one (**6e**).* Pale yellow solid, yield 48%, R_f value 0.40 (CH_2Cl_2/MeOH, 20:1). ^1H NMR (500 MHz, DMSO-d_6) δ 10.65 (s, 1H), 8.33 (s, 1H), 8.30 (s, 1H), 7.92−7.99 (m, 3H), 7.86−7.81 (m, 1H), 7.65 (d, J = 8.5 Hz, 1H), 7.57−7.51 (m, 2H), 6.85 (dd, J = 8.5, 2.3 Hz, 1H), 6.79 (d, J = 2.3 Hz, 1H). ^{13}C NMR (126 MHz, DMSO) δ 161.8, 160.7, 155.5, 142.0, 142.0, 133.2, 133.1, 132.9, 130.6, 128.6, 128.0, 127.7, 127.7, 126.9, 126.6, 122.4, 113.9, 112.6, 102.2. HRMS, calculated for $C_{19}H_{13}O_3$ $[M + H]^+$: 289.0859, found 289.0855.

*7-Hydroxy-3-(3-methoxyphenyl)-2H-chromen-2-one (**6f**).* Pale yellow solid, yield 49%, R_f value 0.30 (CH_2Cl_2/MeOH, 20:1). ^1H NMR (500 MHz, DMSO-d_6) δ 10.64 (s, 1H), 8.19 (s, 1H), 7.61 (d, J = 8.5 Hz, 1H), 7.36 (t, J = 8.2 Hz, 1H), 7.30−7.25 (m, 2H), 6.98−6.94 (m, 1H), 6.83 (dd, J = 8.5, 2.2 Hz, 1H), 6.76 (d, J = 2.1 Hz, 1H), 3.80 (s, 3H). ^{13}C NMR (126 MHz, DMSO) δ 161.8, 160.4, 159.5, 155.4, 141.7, 136.9, 130.5, 129.7, 122.4, 121.1, 114.4, 114.0, 113.9, 112.4, 102.2, 55.6. HRMS, calculated for $C_{16}H_{13}O_4$ $[M + H]^+$: 269.0808, found 269.0806.

*7-Hydroxy-3-(2-methoxyphenyl)-2H-chromen-2-one (**6g**).* Pale yellow solid, yield 32%, R_f value 0.30 (CH_2Cl_2/MeOH, 20:1). ^1H NMR (500 MHz, DMSO-d_6) δ 10.57 (s, 1H), 7.88 (s, 1H), 7.54 (d, J = 8.5 Hz, 1H), 7.42−7.34 (m, 1H), 7.29 (dd, J = 7.4, 1.6 Hz, 1H), 7.08 (d, J = 8.3 Hz, 1H), 7.00 (t, J = 7.4 Hz, 1H), 6.80 (dd, J = 8.3, 2.3 Hz, 1H), 6.75 (d, J = 2.1 Hz, 1H), 3.74 (s, 3H). ^{13}C NMR (126 MHz, DMSO) δ 161.0, 159.6, 157.0, 155.0, 142.4, 130.8, 129.8, 129.7, 124.5, 121.2, 120.2, 113.2, 111.6, 111.4, 101.9, 55.6. HRMS, calculated for $C_{16}H_{13}O_4$ $[M + H]^+$: 269.0808, found 269.0807.

*3-(3-Chlorophenyl)-7-hydroxy-2H-chromen-2-one (**6h**).* Pale yellow solid, yield 47%, R_f value 0.30 (CH_2Cl_2/MeOH, 20:1). ^1H NMR (500 MHz, DMSO-d_6) δ 10.68 (s, 1H), 8.26 (s, 1H), 7.78 (t, J = 1.8 Hz, 1H), 7.68 (dt, J = 7.4, 1.5 Hz, 1H), 7.61 (d, J = 8.5 Hz, 1H), 7.49−7.42 (m, 2H), 6.84 (dd, J = 8.5, 2.3 Hz, 1H), 6.76 (d, J = 2.2 Hz, 1H). ^{13}C NMR (126 MHz, DMSO) δ 162.1, 160.3, 155.5, 142.4, 137.6, 133.3, 130.7, 130.5, 128.4, 128.3, 127.3, 121.0, 114.0, 112.3, 102.2. HRMS, calculated for $C_{15}H_{10}O_3Cl$ $[M + H]^+$: 273.0313, found 273.0310.

*3-(2-Chlorophenyl)-7-hydroxy-2H-chromen-2-one (**6i**).* Pale yellow solid, yield 45%, R_f value 0.30 (CH_2Cl_2/MeOH, 20:1). ^1H NMR (500 MHz, DMSO-d_6) δ 10.68 (s, 1H), 8.00 (d, J = 1.7 Hz, 1H), 7.59 (d, J = 8.5 Hz, 1H), 7.57−7.53 (m, 1H), 7.51−7.39 (m, 3H), 6.84 (dd, J = 8.5, 1.6 Hz, 1H), 6.79 (d, J = 2.0 Hz, 1H). ^{13}C NMR (126 MHz, DMSO) δ 162.0, 159.7, 155.8, 143.9, 143.9, 134.9, 133.4, 132.4, 130.5, 129.8, 127.7, 122.1, 113.9, 111.8, 102.4. HRMS, calculated for $C_{15}H_{10}O_3Cl$ $[M + H]^+$: 273.0313, found 273.0312.

*3-(4-Fluorophenyl)-7-hydroxy-2H-chromen-2-one (**6j**).* Pale yellow solid, yield 38%, R_f value 0.30 (CH_2Cl_2/MeOH, 20:1). ^1H NMR (500 MHz, DMSO-d_6) δ 10.63 (s, 1H), 8.17 (s, 1H), 7.75 (dd, J = 8.9, 5.5 Hz, 2H), 7.61 (d, J = 8.5 Hz, 1H), 7.29 (t, J = 8.9 Hz, 2H), 6.84 (dd, J = 8.5, 2.3 Hz, 1H), 6.77 (d, J = 2.1 Hz, 1H). ^{13}C NMR (126 MHz, DMSO) δ 162.3 (d, J = 245.1 Hz), 161.7, 160.6, 155.4, 141.6, 131.9 (d, J = 3.2 Hz), 130.9, 130.5, 121.6, 115.5 (d, J = 21.4 Hz), 113.9, 112.4, 102.2 (d, J = 8.0 Hz). HRMS, calculated for $C_{15}H_{10}O_3F$ $[M + H]^+$: 257.0605, found 257.0607.

*3-(4-Bromophenyl)-7-hydroxy-2H-chromen-2-one (**6k**).* Brown solid, yield 76%, R_f value 0.30 (CH_2Cl_2/MeOH, 20:1). ^1H NMR (500 MHz, DMSO-d_6) δ 10.70 (s, 1H), 8.21 (s, 1H), 7.69−7.58 (m, 5H), 6.83 (dd, J = 8.5, 2.2 Hz, 1H), 6.75 (d, J = 2.0 Hz, 1H). ^{13}C NMR (126 MHz, DMSO) δ 161.5, 159.9, 155.0, 141.5, 134.3, 131.1, 130.3, 130.2, 121.3, 120.9, 113.5, 111.9, 101.8. HRMS, calculated for $C_{15}H_{10}O_3Br$ $[M + H]^+$: 316.9813, found 316.9806.

*7-Hydroxy-3-(4-iodophenyl)-2H-chromen-2-one (**6l**).* Brown solid, yield 44%, R_f value 0.35 (CH_2Cl_2/MeOH, 20:1). ^1H NMR (500 MHz, DMSO-d_6) δ 10.67 (s, 1H), 8.20 (s, 1H), 7.80 (d, J = 8.4 Hz, 2H), 7.60 (d, J = 8.5 Hz, 1H), 7.52 (d, J = 8.4 Hz, 2H), 6.83 (dd, J = 8.5, 2.2 Hz, 1H), 6.75 (d, J = 2.0 Hz, 1H). ^{13}C NMR (126 MHz, DMSO) δ 161.9, 160.3, 155.5, 141.8, 137.5, 137.4, 135.1, 130.8, 121.5, 114.0, 112.4, 102.2, 94.8. HRMS, calculated for $C_{15}H_{10}O_3Br$ $[M + H]^+$: 364.9670, found 364.9659.

4′-(7-Hydroxy-2-oxo-2*H*-chromen-3-yl)-[1,1′-biphenyl]-4-carboxylic Acid (7). To a suspension of **6l** (190 mg, 0.5 mmol) in EtOH (5 mL), 4-boronobenzoic acid (160 mg, 1.0 mmol) was added. It was followed by addition of $Pd(AcO)_2$ (11 mg, 0.05 mmol) and Na_2CO_3 (210 mg, 2.0 mmol). The mixture was stirred at room temperature for 48 h. The resulting dark brown suspension was filtered through celite and washed with methanol (20 mL). The filtrate was condensed and purified by chromatography with 5% (v/v) MeOH in CH_2Cl_2 to provide the product as a brown solid (110 mg), yield 59%, R_f value 0.45 (CH_2Cl_2/MeOH, 10:1). ^1H NMR (500 MHz, DMSO-d_6) δ 12.98 (s, 1H), 10.66 (s, 1H), 8.26 (s, 1H), 8.04 (d, J = 8.3 Hz, 2H), 7.87−7.81 (m, 6H), 7.63 (d, J = 8.6 Hz, 1H), 6.84 (dd, J = 8.5, 2.1 Hz, 1H), 6.77 (d, J = 1.9 Hz, 1H). ^{13}C NMR (126 MHz, DMSO) δ 167.6, 161.8, 160.5, 155.4, 144.1, 141.6, 138.9, 135.5, 130.6, 130.5, 130.2, 129.3, 127.2, 121.9, 113.9, 112.5, 102.2, 102.2. HRMS, calculated for $C_{22}H_{15}O_5$ $[M + H]^+$: 359.0914, found 359.0912.

3-(3,4-Dimethoxyphenyl)-7-hydroxy-3,4-dihydro-2*H*-benzo[*e*][1,3]oxazin-2-one (8). Compound **8** was synthesized using a reported method.[37] Compound **5** (200 mg, 0.8 mmol) and 3,4-dimethoxyaniline (120 mg, 0.8 mmol) were dissolved in 5 mL of ethanol and stirred at room temperature for 1 h. The suspension turned into deep yellow. With an ice-bath, $NaBH_4$ (50 mg, 1.5 mmol) was added portionwise to the reaction mixture and the resulting mixture was stirred at room temperature for 1 h until the suspension turned into transparent. Subsequently, H_2O (15 mL) was poured into the mixture and extracted with DCM (20 mL × 3). The organic layer was dried over $MgSO_4$. After filtration, the solution was concentrated to 5 mL. Then, carbonyldiimidazole (160 mg, 1 mmol) was added, and the mixture stirred for 16 h at room temperature. DCM (20 mL) was added to dilute the mixture. Then, the mixture was washed with HCl solution (1 N, 20 mL), a saturated $NaHCO_3$ solution (20 mL), and brine (20 mL), dried over $MgSO_4$, and concentrated under vacuum. The residue was dissolved in 5 mL of THF, and tetra-*n*-butylammonium fluoride (260 mg, 1 mmol) was added and stirred at room temperature for 2 h. The resulting mixture was purified with column chromatography using petroleum ether/ethyl acetate 4:1 (v/v) as the eluent. R_f of **8** is 0.2 with petroleum ether/ethyl acetate 2:1 (v/v). ^1H NMR (500 MHz, DMSO-d_6) δ 9.79 (s, 1H), 7.11−7.05 (m, 2H), 7.01−6.94 (m, 2H), 6.60 (dd, J = 8.3, 2.3 Hz, 1H), 6.48 (d, J = 2.2 Hz, 1H), 4.73 (s, 2H), 3.78 (s, 3H), 3.75 (s, 3H). ^{13}C NMR (126 MHz, DMSO) δ 158.3, 150.6, 150.1, 149.3, 148.1, 135.6, 127.0, 118.4, 112.1, 110.8, 109.3, 102.6, 102.5, 56.2, 56.1, 50.5.

(*E*)-2-Fluoro-4-((2-(4-methoxyphenyl)hydrazineylidene)-methyl)phenol (11). To synthesize **11**, 4-methoxybenzohydrazide (254 mg, 1.53 mmol) and 3-fluoro-4-hydroxybenzaldehyde (236 mg, 1.68 mmol) were dissolved in methanol (10 mL). After overnight refluxing, the solvent was evaporated to dryness under reduced pressure and the product was purified using column chromatography (DCM/MeOH 9.5:0.5 to 9:1). The product was isolated as a yellow, crystalline solid (419 mg, 1.45 mmol, 95% yield). qHNMR purity: 96 wt %. M.p.: 229−232 °C. ^1H NMR (600 MHz, DMSO-d_6) δ 11.63 (s, 1H), 10.37 (br. s, 1H), 8.34 (s, 1H), 7.91 (d, J = 8.9 Hz, 2H), 7.49 (d,

https://dx.doi.org/10.1021/acs.jmedchem.0c01160
J. Med. Chem. 2020, 63, 11920−11933

J = 12.0 Hz, 1H), 7.36 (d, J = 8.1 Hz, 1H), 7.06 (d, J = 8.9 Hz, 2H), 7.03 (t, J = 8.6 Hz, 1H), 3.84 (s, 3H). ^{13}C NMR (151 MHz, DMSO-d_6) δ 162.4, 161.9, 151.2 (d, J = 241.8 Hz), 146.8 (d, J = 11.9 Hz), 146.3, 129.4, 126.3 (d, J = 6.1 Hz), 125.5, 124.2, 117.9 (d, J = 3.2 Hz), 113.9 (d, J = 18.9 Hz,), 113.7, 55.4. ^{19}F NMR (565 MHz, DMSO-d_6) δ −137.37 (t, J = 10.5 Hz). HRMS calculated for $C_{15}H_{14}FN_2O_3$ $[M + H]^+$: 289.098, found 289.098.

Preparation of Human MIF and MBP−sCD74. C-terminal His-tagged recombinant human MIF was expressed through transforming a pET-20b(+) plasmid containing the target gene into *Escherichia coli* BL21 (DE3) according to literature procedures.[60] Overexpression was performed by following a protocol as described in a previous study.[52] Cells were collected and resuspended into buffer A containing 20 mM Tris-HCl (pH 7.5), 20 mM NaCl, 2 mM $MgCl_2$, and 10% (v/v) glycerol 0.2× complete EDTA-free protease inhibitor cocktail (Roche). After sonication, the insoluble material was removed by centrifugation at 17,000g for 20 min. The obtained supernatant was applied to a medium-pressure chromatography system (Biologic Duoflow) equipped with a His trap HP (5 mL) column with detection at 280 nm for the eluent. The column was washed with a binding buffer containing 50 mM Tris and 10% glycerol at pH 7.4 and eluted with an elution buffer containing 500 mM imidazole, 50 mM Tris, and 10% glycerol at pH 7.4. The pure fractions (as judged by SDS-PAGE) were pooled and subjected to a PD-10 column (GE Healthcare) that was equilibrated with PBS buffer at pH 7.4 to remove the high concentration of imidazole. The collected MIF solution was divided into 50 μL aliquots and stored at −80 °C.

To express human CD74 fusion protein, the pET20b−MBP−sCD74 plasmid was transformed into Rossetta-gami 2 (DE3) using previously described procedures.[52] After having obtained the cell-free extract, MBP−sCD74 was first purified with a His trap HP (5 mL, GE Healthcare) column on a medium-pressure chromatography system (Biologic Duoflow) with detection at 280 nm for the eluent. The column was washed with a binding buffer containing 50 mM Tris and 10% glycerol at pH 7.4 and eluted with an elution buffer containing 500 mM imidazole, 50 mM Tris, and 10% glycerol at pH 7.4. The pure fractions (as judged by SDS-PAGE) were pre-equilibrated with buffer A (50 mM Tris-HCl, 10% glycerol, pH 7.4) and incubated with 5 mL of MBPTrap resin (GE Healthcare) in a gravity column at 4 °C with rotation overnight. This was followed by removing the nonbound proteins with 50 mL of buffer A by gravity flow. Bound protein was eluted with 15 mL of buffer B (50 mM Tris-HCl, 10 mM maltose, 10% glycerol, pH 7.4). The collected fractions were analyzed by SDS-PAGE, and the pure fractions were pooled and then divided into 50 μL aliquots and stored at −80 °C.

Enzyme Assays. The protocol for measuring inhibition of MIF tautomerase enzyme activity and enzyme kinetics was adapted from our previous protocol.[35] In brief, 180 μL of a 500 nM MIF solution in boric acid buffer (435 mM, pH 6.2) was mixed with 10 μL of a 20 mM EDTA solution in demineralized water and 10 μL of a solution of the desired compound dissolved in DMSO or blank DMSO. This mixture was preincubated at room temperature for 10 min. Next, 50 μL of this mixture was mixed with 50 μL of a 1 mM 4-HPP solution in ammonium acetate buffer (50 mM, pH 6.0). Subsequently, MIF tautomerase activity was monitored by measuring the increase of UV absorbance at 306 nm over time. MIF tautomerase activity in the presence a blank DMSO dilution was set to 100% enzyme activity. Noncatalyzed conversion of the substrate in the absence of MIF was set to 0%. Data from the first 3 min were used to calculate the initial velocities. All experiments were repeated three times, and calculations were performed with the program GraphPad Prism.

UV−vis and Fluorescence Spectra Measurements. UV−vis absorbance and fluorescence spectra were recorded on a Synergy H1 Hybrid Reader (BioTek) instrument. UV absorption spectra of the coumarin derivatives were measured at 100 μM of the respective compound in PBS buffer (pH 7.4) containing 5% (v/v) DMSO in transparent 96-well plates (#655801, Greiner). Fluorescence emission spectra were measured in 200 μL of a 200 nM solution of the respective compound in PBS (pH 7.4) containing 5% (v/v) DMSO (pH 7.4 PBS) in 96-well plates (#655900, Greiner). The excitation wavelength was set to 340 nm for **6d** and to 355 nm for **7** to measure the emission spectra from 380 to 600 nm. The excitation and emission slit widths were both 5 nm.

K_S Determination of 6d and 7. To determine the binding affinity K_S of **6d**, a solution of **6d** (200 nM) was prepared by diluting a 10 mM solution of **6d** in DMSO with PBS buffer (pH 7.4). A dilution series (16−8000 nM) of MIF in PBS buffer (pH 7.4) was freshly prepared. Subsequently, 100 μL of the **6d** solution (200 nM) was mixed with 100 μL of the MIF dilutions followed by 10 min of incubation at room temperature. The fluorescence intensity was monitored at Ex/Em = 340/460 nm in a 96-well plate (#655900, Greiner). The specific equilibrium binding constant (K_S) was derived from the specific binding curve by fitting the data to a hyperbolic curve using GraphPad Prism. K_S of **7** was obtained using the same protocol except that fluorescence intensity was measured at Ex/Em = 355/455 nm.

FID Assays of Representative Nonfluorescent Inhibitors. This assay was performed according to the workflow shown in Figure S10. A solution of each test compound (various concentrations in 50 μL of pH 7.4 PBS buffer containing 5 μL of DMSO) was incubated with MIF (200 nM in 100 μL of pH 7.4 PBS buffer) at room temperature for 10 min. Next, **7** (200 nM in 50 μL of pH 7.4 PBS buffer) was added into the mixture and incubated at room temperature for another 10 min. The final concentrations in each well were 100 nM for MIF, 50 nM for indicator **7**, 2.5% (v/v) for DMSO, and various concentrations for the tested inhibitors. Fluorescence intensity was measured at Ex/Em = 355/455 nm in a 96-well plate (#655900, Greiner). Calculation of EC_{50} was carried out with GraphPad Prism.

Docking Study. Docking studies were performed to gain insight into SARs. All molecular modeling studies were done with the program Discovery Studio (Dassault Systèmes) version 2018, and the crystal structures of human recombinant MIF (PDB code: 1GCZ)[43] was used. The CDOCKER protocol was used for docking, which is a CHARMM-based algorithm. Docking was verified by use of the ligand ethyl 7-hydroxy-2-oxo-2*H*-chromene-3-carboxylate (Orita-1) from the crystal structure 1GCZ. All 10 highest ranked poses show a comparable position to the original pose of **2** (Orita-1) from the crystal structure in the 7-hydroxycoumarin functionality (Figure S7). Poses with the lowest CDOCKER energies were chosen for representation.

ELISA. Freshly thawed MIF (stored at −80 °C) aliquots were diluted in PBS buffer (pH 7.4) to a concentration of 250 nM. 100 μL of this solution was used for coating of the wells of a high-binding 96-well plate overnight at 4 °C. The wells were washed three times with 220 μL of washing buffer (PBS with 0.05% Tween20) and subsequently blocked with 210 μL of freshly prepared 2% (w/v) bovine serum albumin solution in PBS buffer at room temperature for 1 h. During all incubation steps, the plate was shaken slowly on a microplate shaker. The blocking solution was removed, and the plate was washed three times with washing buffer. Subsequently, a solution of the inhibitor (2 μL in DMSO) was mixed with an sCD74 solution (510 nM, 98 μL in PBS buffer (pH 7.4) to obtain a 100 μL mixture with 500 nM sCD74 and an inhibitor concentration ranging from 1 to 100 μM. After 10 min of incubation at room temperature, the inhibitor−sCD74 mixtures were added to each well and incubated for 30 min at room temperature. At this step, a blank DMSO dilution was used as vehicle control. PBS buffer (100 μL) without sCD74 was used as control to exclude the nonspecific binding of anti-CD74 pAb. After washing, the wells were incubated with 100 μL of a rabbit anti-CD74 pAb solution (1:1000 dilution in PBS, 0.2% BSA) (Sinobiological, The Netherlands) at room temperature for 30 min. After removing the anti-CD74 solution and washing, a solution of 100 μL of goat anti-rabbit horseradish peroxidase conjugate (1:1000 dilution in PBS, 0.2% BSA) (Life Technologies, The Netherlands) was added and incubated at room temperature for 30 min. After washing, binding was visualized by conversion of 100 μL of aqueous tetramethylbenzydine (TMB) solution (Sigma Aldrich, The Netherlands), which was quenched with an aqueous 1 N H_2SO_4 solution (100 μL). The UV absorbance was

https://dx.doi.org/10.1021/acs.jmedchem.0c01160
J. Med. Chem. 2020, 63, 11920−11933

detected at 450 nm. Data were analyzed with the program GraphPad Prism.

Colony Formation Assay. A549 cells were seeded in 6-well plates (100 cells per well in 2 mL of RPMI medium (#61970-010, Gibco) containing 10% (v/v) fetal bovine serum (FBS) and 100 U/mL penicillin/streptomycin (#10378016, Gibco)) and incubated overnight. Stock solutions (10 mM) of inhibitors were prepared using DMSO as solvent. The cells were treated with corresponding inhibitors for 10 days. Subsequently, the medium was carefully removed, and cells were fixed with 4% (v/v) paraformaldehyde for 20 min and stained with 0.5% (w/v) crystal violet for 20 min. After washing, the image of each well was photographed and analyzed with ImageJ. We defined one colony as an aggregate of >50 cells. The final concentration of DMSO was 0.2% for this assay. The 0.2% DMSO-treated group was used as vehicle control.

ERK Signaling Pathway Study. A549 cells (2×10^5 cells per well) were seeded into each well of a 6-well plate with 2 mL of RPMI-1640 medium containing 10% FBS (Costar Europe, Badhoevedorp, The Netherlands) and 1% penicillin/streptomycin solution (Corning). After overnight culturing, the medium was removed. In the experimental groups, a fresh medium with 150 ng/mL MIF (endotoxin-free) and different concentrations of **7** was added to cells. A fresh medium containing 150 ng/mL MIF was applied as the positive control. The medium was used as negative control. DMSO concentration was 0.2% for all groups. After that, cells were lysed with a RIPA buffer containing 1× PhosSTOP and protease inhibitor (PI) cocktail (Roche, Mannheim, Germany). The BCA Protein Assay Kit (Pierce, Rockford, IL, USA) was used to determine the protein concentration. 30 μg of protein was separated by a precast 10% NuPAGE Bis-Tris gel (Invitrogen, USA) and then transferred to a polyvinylidene difluoride (PVDF) membrane. Five percent of skimmed milk was used to block the membrane for 1 h at room temperature. The blocked membrane was incubated with an appropriate primary antibody (pERK, #9101, Cell Signaling, 1:1000; GAPDH, #97166, Cell Signaling, 1:10000) overnight at 4 °C followed by the treatment of an HRP-conjugated secondary goat anti-rabbit antibody (#P0448, Dako, 1:2000) or rabbit anti-mouse antibody (#P0260, Dako, 1:2000) at room temperature for 1 h. The protein bands were visualized with enhanced chemiluminescence (ECL) solution (GE Healthcare). The figures were quantified with ImageJ software based on grayscale.

■ ASSOCIATED CONTENT

Supporting Information

The Supporting Information is available free of charge at https://pubs.acs.org/doi/10.1021/acs.jmedchem.0c01160.

Dose−inhibition curves, fluorescence quantum yield measurement, active site titration of MIF, fluorescence decay profile of **7**, kinetics study of **7**, influence of copper ions on the FID assay, dose−response curves of MIF inhibitors, comparison of FID and 4-HPP tautomerization assays, ELISA of MIF inhibitors, cell viability assay of **7**; HPLC assessment of purity and solubility for target compounds; tautomerase activity inhibition IC_{50} curves; molecular modeling details; analytical data (^{1}H NMR, ^{13}C NMR, HRMS) (PDF)

Molecular formula strings (CSV)

Docking studies with the ligand ethyl 7-hydroxy-2-oxo-2*H*-chromene-3-carboxylate (PDB)

■ AUTHOR INFORMATION

Corresponding Author

Frank J. Dekker − *Chemical and Pharmaceutical Biology, Groningen Research Institute of Pharmacy (GRIP), University of Groningen, 9713 AV Groningen, The Netherlands;* orcid.org/0000-0001-7217-9300; Phone: +31-5-3638030; Email: f.j.dekker@rug.nl; Fax: +31-5-3637953

Authors

Zhangping Xiao − *Chemical and Pharmaceutical Biology, Groningen Research Institute of Pharmacy (GRIP), University of Groningen, 9713 AV Groningen, The Netherlands*

Deng Chen − *Chemical and Pharmaceutical Biology, Groningen Research Institute of Pharmacy (GRIP), University of Groningen, 9713 AV Groningen, The Netherlands*

Shanshan Song − *Chemical and Pharmaceutical Biology, Groningen Research Institute of Pharmacy (GRIP) and Molecular Pharmacology, Groningen Research Institute of Pharmacy (GRIP), University of Groningen, 9713 AV Groningen, The Netherlands*

Ramon van der Vlag − *Stratingh Institute for Chemistry, University of Groningen, 9747 AG Groningen, the Netherlands;* orcid.org/0000-0002-8796-2792

Petra E. van der Wouden − *Chemical and Pharmaceutical Biology, Groningen Research Institute of Pharmacy (GRIP), University of Groningen, 9713 AV Groningen, The Netherlands*

Ronald van Merkerk − *Chemical and Pharmaceutical Biology, Groningen Research Institute of Pharmacy (GRIP), University of Groningen, 9713 AV Groningen, The Netherlands*

Robbert H. Cool − *Chemical and Pharmaceutical Biology, Groningen Research Institute of Pharmacy (GRIP), University of Groningen, 9713 AV Groningen, The Netherlands*

Anna K. H. Hirsch − *Stratingh Institute for Chemistry, University of Groningen, 9747 AG Groningen, the Netherlands; Department of Drug Design and Optimization, Helmholtz Institute for Pharmaceutical Research Saarland (HIPS) − Helmholtz Centre for Infection Research (HZI) Campus Building E8.1, 66123 Saarbrücken, Germany; Department of Pharmacy, Saarland University, 66123 Saarbrücken, Germany;* orcid.org/0000-0001-8734-4663

Barbro N. Melgert − *Molecular Pharmacology, Groningen Research Institute of Pharmacy (GRIP), University of Groningen, 9713 AV Groningen, The Netherlands; Groningen Research Institute of Asthma and COPD, University Medical Center Groningen, University of Groningen, 9713 GZ Groningen, The Netherlands*

Wim J. Quax − *Chemical and Pharmaceutical Biology, Groningen Research Institute of Pharmacy (GRIP), University of Groningen, 9713 AV Groningen, The Netherlands;* orcid.org/0000-0002-5162-9947

Gerrit J. Poelarends − *Chemical and Pharmaceutical Biology, Groningen Research Institute of Pharmacy (GRIP), University of Groningen, 9713 AV Groningen, The Netherlands;* orcid.org/0000-0002-6917-6368

Complete contact information is available at: https://pubs.acs.org/10.1021/acs.jmedchem.0c01160

Author Contributions

All authors have given approval to the final version of the manuscript.

Funding

Z.X. and D.C. are funded by the China Scholarship Council. S.S. is funded by the Royalties Prof. Dr. H.W. Frijlink Scholarship from University of Groningen.

Notes

The authors declare no competing financial interest.

■ ACKNOWLEDGMENTS

We acknowledge Professor Wesley R. Browne from Molecular Inorganic Chemistry-Stratingh Institute for Chemistry, University of Groningen for advice and help in performing the fluorescence lifetime assays.

■ ABBREVIATIONS

4-HPP, 4-hydroxylphenylpyruvate; CD74, cluster of differentiation 74; CXCR4, chemokine receptor 4; DMF, *N*,*N*-dimethylformamide; EDCI, 1-ethyl-3-(3-dimethylaminopropyl)carbodiimide hydrochloride; EDTA, ethylenediaminetetraacetic acid; ELISA, enzyme-linked immunosorbent assay; FID, fluorescent indicator displacement; HTS, high-throughput screening; HOBt, hydroxybenzotriazole; MAPK, mitogen-activated protein kinase; MIF, macrophage migration inhibitory factor; NMM, *N*-methylmorpholine; TBAF, tetrabutylammonium fluoride; TBDMS, *tert*-butyldimethylsilyl; THF, tetrahydrofuran

■ REFERENCES

(1) Bray, F.; Ferlay, J.; Soerjomataram, I.; Siegel, R. L.; Torre, L. A.; Jemal, A. Global cancer statistics 2018: GLOBOCAN estimates of incidence and mortality worldwide for 36 cancers in 185 countries. *Ca-Cancer J. Clin.* **2018**, *68*, 394−424.

(2) Vasan, N.; Baselga, J.; Hyman, D. M. A view on drug resistance in cancer. *Nature* **2019**, *575*, 299−309.

(3) Bilsborrow, J. B.; Doherty, E.; Tilstam, P. V.; Bucala, R. Macrophage migration inhibitory factor (MIF) as a therapeutic target for rheumatoid arthritis and systemic lupus erythematosus. *Expert Opin. Ther. Targets* **2019**, *23*, 733−744.

(4) Sinitski, D.; Kontos, C.; Krammer, C.; Asare, Y.; Kapurniotu, A.; Bernhagen, J. Macrophage migration inhibitory factor (MIF)-based therapeutic concepts in atherosclerosis and inflammation. *Thromb. Haemostasis* **2019**, *119*, 553−566.

(5) Bucala, R.; Donnelly, S. C. Macrophage migration inhibitory factor: a probable link between inflammation and cancer. *Immunity* **2007**, *26*, 281−285.

(6) Guda, M. R.; Rashid, M. A.; Asuthkar, S.; Jalasutram, A.; Caniglia, J. L.; Tsung, A. J.; Velpula, K. K. Pleiotropic role of macrophage migration inhibitory factor in cancer. *Am. J. Cancer Res.* **2019**, *9*, 2760−2773.

(7) Penticuff, J. C.; Woolbright, B. L.; Sielecki, T. M.; Weir, S. J.; Taylor, J. A. MIF family proteins in genitourinary cancer: tumorigenic roles and therapeutic potential. *Nat. Rev. Urol.* **2019**, *16*, 318−328.

(8) Soumoy, L.; Kindt, N.; Ghanem, G.; Saussez, S.; Journe, F. Role of macrophage migration inhibitory factor (Mif) in melanoma. *Cancers (Basel).* **2019**, *11*, 1−11.

(9) Cavalli, E.; Ciurleo, R.; Petralia, M. C.; Fagone, P.; Bella, R.; Mangano, K.; Nicoletti, F.; Bramanti, P.; Basile, M. S. Emerging role of the macrophage migration inhibitory factor family of cytokines in neuroblastoma. Pathogenic effectors and novel therapeutic targets? *Molecules* **2020**, *25*, 1−19.

(10) Coleman, A. M.; Rendon, B. E.; Zhao, M.; Qian, M.-W.; Bucala, R.; Xin, D.; Mitchell, R. A. Cooperative regulation of non-small cell lung carcinoma angiogenic potential by macrophage migration inhibitory factor and its homolog, D-dopachrome tautomerase. *J. Immunol.* **2008**, *181*, 2330−2337.

(11) Kindt, N.; Journe, F.; Laurent, G.; Saussez, S. Involvement of macrophage migration inhibitory factor in cancer and novel therapeutic targets. *Oncol. Lett.* **2016**, *12*, 2247−2253.

(12) Nobre, C. C. G.; de Araújo, J. M. G.; Fernandes, T. A. A. d. M.; Cobucci, R. N. O.; Lanza, D. C. F.; Andrade, V. S.; Fernandes, J. V. Macrophage migration inhibitory factor (MIF): biological activities and relation with cancer. *Pathol. Oncol. Res.* **2017**, *23*, 235−244.

(13) Balogh, K. N.; Templeton, D. J.; Cross, J. V. Macrophage migration inhibitory factor protects cancer cells from immunogenic cell death and impairs anti-tumor immune responses. *PLoS One* **2018**, *13*, 1−20.

(14) Oliveira, C. S.; de Bock, C. E.; Molloy, T. J.; Sadeqzadeh, E.; Geng, X. Y.; Hersey, P.; Zhang, X. D.; Thorne, R. F. Macrophage migration inhibitory factor engages PI3K/Akt signalling and is a prognostic factor in metastatic melanoma. *BMC Cancer* **2014**, *14*, 1−14.

(15) Leng, L.; Metz, C. N.; Fang, Y.; Xu, J.; Donnelly, S.; Baugh, J.; Delohery, T.; Chen, Y.; Mitchell, R. A.; Bucala, R. MIF signal transduction initiated by binding to CD74. *J. Exp. Med.* **2003**, *197*, 1467−1476.

(16) Shi, X.; Leng, L.; Wang, T.; Wang, W.; Du, X.; Li, J.; McDonald, C.; Chen, Z.; Murphy, J. W.; Lolis, E.; Noble, P.; Knudson, W.; Bucala, R. CD44 is the signaling component of the macrophage migration inhibitory factor-CD74 receptor complex. *Immunity* **2006**, *25*, 595−606.

(17) Kleemann, R.; Hausser, A.; Geiger, G.; Mischke, R.; Burger-kentischer, A.; Flieger, O.; Johannes, F.; Roger, T.; Calandra, T.; Kapurniotu, A. Intracellular action of the cytokine MIF to modulate AP-1 activity and the cell cycle through Jab1. *Nature* **2000**, *408*, 211−216.

(18) Mitchell, R. A.; Liao, H.; Chesney, J.; Fingerle-Rowson, G.; Baugh, J.; David, J.; Bucala, R. Macrophage migration inhibitory factor (MIF) sustains macrophage proinflammatory function by inhibiting p53: Regulatory role in the innate immune response. *Proc. Natl. Acad. Sci.* **2002**, *99*, 345−350.

(19) Mahalingam, D.; Patel, M.; Sachdev, J.; Hart, L.; Halama, N.; Ramanathan, R.; Sarantopoulos, J.; Liu, X.; Yazji, S.; Jäger, D.; Adib, D.; Kerschbaumer, R.; Yoon, M.; Manzur, G.; Starodub, A.; Sivarajan, K.; Wertheim, M.; Thambi, P.; Jones, M.; Goel, S.; Nemunaitis, J.; Tsimberidou, A. Safety and efficacy analysis of imalumab, an anti-oxidized macrophage migration inhibitory factor (oxMIF) antibody, alone or in combination with 5-fluorouracil/leucovorin (5-FU/LV) or panitumumab, in patients with metastatic colorectal cancer (mCRC). *Ann. Oncol.* **2016**, *27*, ii105.

(20) Trivedi-Parmar, V. C.; Jorgensen, W. L. Advances and insights for small molecule inhibition of macrophage migration inhibitory factor. *J. Med. Chem.* **2018**, *61*, 8104−8119.

(21) Kok, T.; Wasiel, A. A.; Cool, R. H.; Melgert, B. N.; Poelarends, G. J.; Dekker, F. J. Small-molecule inhibitors of macrophage migration inhibitory factor (MIF) as an emerging class of therapeutics for immune disorders. *Drug Discovery Today* **2018**, *23*, 1910−1918.

(22) Sun, H. W.; Bernhagen, J.; Bucala, R.; Lolis, E. Crystal structure at 2.6-A resolution of human macrophage migration inhibitory factor. *Proc. Natl. Acad. Sci.* **1996**, *93*, 5191−5196.

(23) Lubetsky, J. B.; Swope, M.; Dealwis, C.; Blake, P.; Lolis, E. Pro-1 of macrophage migration inhibitory factor functions as a catalytic base in the phenylpyruvate tautomerase activity. *Biochemistry* **1999**, *38*, 7346−7354.

(24) Pantouris, G.; Syed, M. A.; Fan, C.; Rajasekaran, D.; Cho, T. Y.; Rosenberg, E. M., Jr.; Bucala, R.; Bhandari, V.; Lolis, E. J. An analysis of MIF structural features that control functional activation of CD74. *Chem. Biol.* **2015**, *22*, 1197−1205.

(25) Assis, D. N.; Leng, L.; Du, X.; Zhang, C. K.; Grieb, G.; Merk, M.; Garcia, A. B.; Mccrann, C.; Chapiro, J.; Meinhardt, A.; Mizue, Y.; Nikolic-Paterson, D. J.; Bernhagen, J.; Kaplan, M. M.; Zhao, H.; Boyer, J. L.; Bucala, R. The role of macrophage migration inhibitory factor in autoimmune liver disease. *Hepatology* **2014**, *59*, 580−591.

(26) Pantouris, G.; Khurana, L.; Ma, A.; Skeens, E.; Reiss, K.; Batista, V. S.; Lisi, G. P.; Lolis, E. J. Regulation of MIF enzymatic activity by an allosteric site at the central solvent channel. *Cell Chem. Biol.* **2020**, *27*, 740−750.e5.

(27) Bloom, J.; Sun, S.; Al-Abed, Y. MIF, a controversial cytokine: a review of structural features, challenges, and opportunities for drug development. *Expert Opin. Ther. Targets* **2016**, *20*, 1463−1475.

(28) Al-Abed, Y.; VanPatten, S. MIF as a disease target: ISO-1 as a proof-of-concept therapeutic. *Future Med. Chem.* **2011**, *3*, 45−63.

(29) Meyer-Siegler, K. L.; Iczkowski, K. A.; Leng, L.; Bucala, R.; Vera, P. L. Inhibition of macrophage migration inhibitory factor or its

https://dx.doi.org/10.1021/acs.jmedchem.0c01160
J. Med. Chem. 2020, 63, 11920−11933

receptor (CD74) attenuates growth and invasion of DU-145 prostate cancer cells. *J. Immunol.* **2006**, *177*, 8730−8739.
(30) Mawhinney, L.; Armstrong, M. E.; O' Reilly, C.; Bucala, R.; Leng, L.; Fingerle-Rowson, G.; Fayne, D.; Keane, M. P.; Tynan, A.; Maher, L.; Cooke, G.; Lloyd, D.; Conroy, H.; Donnelly, S. C. Macrophage migration inhibitory factor (MIF) enzymatic activity and lung cancer. *Mol. Med.* **2014**, *20*, 729−735.
(31) Varinelli, L.; Caccia, D.; Volpi, C. C.; Caccia, C.; De Bortoli, M.; Taverna, E.; Gualeni, A. V.; Leoni, V.; Gloghini, A.; Manenti, G.; Bongarzone, I. 4-IPP, a selective MIF inhibitor, causes mitotic catastrophe in thyroid carcinomas. *Endocr.-Relat. Cancer* **2015**, *22*, 759−775.
(32) Olivares, C.; Jiménez-Cervantes, C.; Lozano, J. A.; Solano, F.; García-Borrón, J. C. The 5,6-dihydroxyindole-2-carboxylic acid (DHICA) oxidase activity of human tyrosinase. *Biochem. J.* **2001**, *354*, 131−139.
(33) Ouertatani-Sakouhi, H.; Liu, M.; El-Turk, F.; Cuny, G. D.; Glicksman, M. A.; Lashuel, H. Kinetic-based high-throughput screening assay to discover novel classes of macrophage migration inhibitory factor inhibitors. *J. Biomol. Screen.* **2010**, *15*, 347−358.
(34) Schlund, S.; Janke, E. M. B.; Weisz, K.; Engels, B. Predicting the tautomeric equilibrium of acetylacetone in solution. I. The right answer for the wrong reason? *J. Comput. Chem.* **2010**, *31*, 665−670.
(35) Xiao, Z.; Fokkens, M.; Chen, D.; Kok, T.; Proietti, G.; van Merkerk, R.; Poelarends, G. J.; Dekker, F. J. Structure-activity relationships for binding of 4-substituted triazole-phenols to macrophage migration inhibitory factor (MIF). *Eur. J. Med. Chem.* **2020**, *186*, 111849−111862.
(36) Cisneros, J. A.; Robertson, M. J.; Valhondo, M.; Jorgensen, W. L. Irregularities in enzyme assays: The case of macrophage migration inhibitory factor. *Bioorg. Med. Chem. Lett.* **2016**, *26*, 2764−2767.
(37) Cisneros, J. A.; Robertson, M. J.; Valhondo, M.; Jorgensen, W. L. A fluorescence polarization assay for binding to macrophage migration inhibitory factor and crystal structures for complexes of two potent inhibitors. *J. Am. Chem. Soc.* **2016**, *138*, 8630−8638.
(38) Lubetsky, J. B.; Dios, A.; Han, J.; Aljabari, B.; Ruzsicska, B.; Mitchell, R.; Lolis, E.; Al-Abed, Y. The tautomerase active site of macrophage migration inhibitory factor is a potential target for discovery of novel anti-inflammatory agents. *J. Biol. Chem.* **2002**, *277*, 24976−24982.
(39) del Villar-Guerra, R.; Gray, R. D.; Trent, J. O.; Chaires, J. B. A rapid fluorescent indicator displacement assay and principal component/cluster data analysis for determination of ligand−nucleic acid structural selectivity. *Nucleic Acids Res.* **2018**, *46*, 1−10.
(40) Yamada, S.; Kawasaki, M.; Fujihara, M.; Watanabe, M.; Takamura, Y.; Takioku, M.; Nishioka, H.; Takeuchi, Y.; Makishima, M.; Motoyama, T.; Ito, S.; Tokiwa, H.; Nakano, S.; Kakuta, H. Competitive binding assay with an umbelliferone-based fluorescent rexinoid for retinoid X receptor ligand screening. *J. Med. Chem.* **2019**, *62*, 8809−8818.
(41) Nguyen, B. T.; Anslyn, E. V. Indicator-displacement assays. *Coord. Chem. Rev.* **2006**, *250*, 3118−3127.
(42) Cao, D.; Liu, Z.; Verwilst, P.; Koo, S.; Jangjili, P.; Kim, J. S.; Lin, W. Coumarin-based small-molecule fluorescent chemosensors. *Chem. Rev.* **2019**, *119*, 10403−10519.
(43) Orita, M.; Yamamoto, S.; Katayama, N.; Aoki, M.; Takayama, K.; Yamagiwa, Y.; Seki, N.; Suzuki, H.; Kurihara, H.; Sakashita, H.; Takeuchi, M.; Fujita, S.; Yamada, T.; Tanaka, A. Coumarin and chromen-4-one analogues as tautomerase inhibitors of macrophage migration inhibitory factor: Discovery and X-ray crystallography. *J. Med. Chem.* **2001**, *44*, 540−547.
(44) Cheng, Y.-C.; Prusoff, W. H. Relationship between the inhibition constant (Ki) and the concentration of inhibitor which causes 50 percent inhibition (IC50) of an enzymatic reaction. *Biochem. Pharmacol.* **1973**, *22*, 3099−3108.
(45) Hargrove, A. E.; Zhong, Z.; Sessler, J. L.; Anslyn, E. V. Algorithms for the determination of binding constants and enantiomeric excess in complex host: Guest equilibria using optical measurements. *New J. Chem.* **2010**, *34*, 348−354.
(46) Morrison, J. F. Kinetics of the reversible inhibition of enzyme-catalysed reactions by tight-binding inhibitors. *Biochim. Biophys. Acta* **1969**, *185*, 269−286.
(47) Dziedzic, P.; Cisneros, J. A.; Robertson, M. J.; Hare, A. A.; Danford, N. E.; Baxter, R. H. G.; Jorgensen, W. L. Design, synthesis, and protein crystallography of biaryltriazoles as potent tautomerase inhibitors of macrophage migration inhibitory factor. *J. Am. Chem. Soc.* **2015**, *137*, 2996−3003.
(48) Zhang, J.-H.; Chung, T. D. Y.; Oldenburg, K. R. A simple statistical parameter for use in evaluation and validation of high throughput screening assays. *J. Biomol. Screen.* **1999**, *4*, 67−73.
(49) Dabideen, D. R.; Cheng, K. F.; Aljabari, B.; Miller, E. J.; Pavlov, V. A.; Al-Abed, Y. Phenolic hydrazones are potent inhibitors of macrophage migration inhibitory factor proinflammatory activity and survival improving agents in sepsis. *J. Med. Chem.* **2007**, *50*, 1993−1997.
(50) Ouertatani-Sakouhi, H.; El-Turk, F.; Fauvet, B.; Roger, T.; Le Roy, D.; Karpinar, D. P.; Leng, L.; Bucala, R.; Zweckstetter, M.; Calandra, T.; Lashuel, H. A. A new class of isothiocyanate-based irreversible inhibitors of macrophage migration inhibitory factor. *Biochemistry* **2009**, *48*, 9858−9870.
(51) Spencer, E. S.; Dale, E. J.; Gommans, A. L.; Rutledge, M. T.; Vo, C. T.; Nakatani, Y.; Gamble, A. B.; Smith, R. A. J.; Wilbanks, S. M.; Hampton, M. B.; Tyndall, J. D. A. Multiple binding modes of isothiocyanates that inhibit macrophage migration inhibitory factor. *Eur. J. Med. Chem.* **2015**, *93*, 501−510.
(52) Kok, T.; Wasiel, A. A.; Dekker, F. J.; Poelarends, G. J.; Cool, R. H. High yield production of human invariant chain CD74 constructs fused to solubility-enhancing peptides and characterization of their MIF-binding capacities. *Protein Expression Purif.* **2018**, *148*, 46−53.
(53) Rendon, B. E.; Roger, T.; Teneng, I.; Zhao, M.; Al-Abed, Y.; Calandra, T.; Mitchell, R. A. Regulation of human lung adenocarcinoma cell migration and invasion by macrophage migration inhibitory factor. *J. Biol. Chem.* **2007**, *282*, 29910−29918.
(54) Koutnik, P.; Shcherbakova, E. G.; Gozem, S.; Caglayan, M. G.; Minami, T.; Anzenbacher, P., Jr. Fluorescence-based assay for carbonic anhydrase inhibitors. *Chem* **2017**, *2*, 271−282.
(55) Cournia, Z.; Leng, L.; Gandavadi, S.; Du, X.; Bucala, R.; Jorgensen, W. L. Discovery of human macrophage migration inhibitory factor (MIF)-CD74 antagonists via virtual screening. *J. Med. Chem.* **2009**, *52*, 416−424.
(56) Hopkins, A. L.; Keserü, G. M.; Leeson, P. D.; Rees, D. C.; Reynolds, C. H. The role of ligand efficiency metrics in drug discovery. *Nat. Rev. Drug Discov.* **2014**, *13*, 105−121.
(57) Vieira, L. C. C.; Paixão, M. W.; Corrêa, A. G. Green synthesis of novel chalcone and coumarin derivatives via Suzuki coupling reaction. *Tetrahedron Lett.* **2012**, *53*, 2715−2718.
(58) Ghalehshahi, H. G.; Balalaie, S.; Aliahmadi, A. Peptides N-connected to hydroxycoumarin and cinnamic acid derivatives: Synthesis and fluorescence spectroscopic, antioxidant and antimicrobial properties. *New J. Chem.* **2018**, *42*, 8831−8842.
(59) Sashidhara, K. V.; Palnati, G. R.; Avula, S. R.; Kumar, A. Efficient and general synthesis of 3-aryl coumarins using cyanuric chloride 1. *Synlett* **2012**, *23*, 611−621.
(60) Bernhagen, J.; Mitchell, R. A.; Calandra, T.; Voelter, W.; Cerami, A.; Bucala, R. Purification, bioactivity, and secondary structure analysis of mouse and human macrophage migration inhibitory factor (MIF). *Biochemistry* **1994**, *33*, 14144−14155.

https://dx.doi.org/10.1021/acs.jmedchem.0c01160
J. Med. Chem. 2020, 63, 11920−11933